Rochester Institute of Technology
RIT Digital Institutional Repository

Theses

2004

# Design and Simulation of a MEMS Long Distance Traveling Micro-Actuator

Younes Elkacimi

Follow this and additional works at: https://repository.rit.edu/theses

Recommended Citation
Elkacimi, Younes, "Design and Simulation of a MEMS Long Distance Traveling Micro-Actuator" (2004). Thesis. Rochester Institute of Technology. Accessed from

This Thesis is brought to you for free and open access by the RIT Libraries. For more information, please contact repository@rit.edu.

# DESIGN AND SIMULATION OF A MEMS LONG DISTANCE TRAVELING MICRO-ACTUATOR

By

**Younes Elkacimi**

**A Thesis Submitted in**
**Partial Fulfillment of the Requirement for the**

## MASTER OF SCIENCE
## IN
## MECHANICAL ENGINEERING

**Approved by:**

**Dr. Mustafa A.G. Abushagur** _____
Microsystems Engineering Ph.D. Program Director and Professor (Thesis Advisor)

**Dr. Lynn F. Fuller** _____
Department of Microelectronic Engineering Motorola Professor

**Dr. Wayne Walter** _____
Department of Mechanical Engineering Professor

**Dr. Edward C. Hensel** _____
Department Head of Mechanical Engineering and Professor

**DEPARTMENT OF MECHANICAL ENGINEERING**
**ROCHESTER INSTITUTE OF TECHNOLOGY**

**August 2004**

# THESIS REPRODUCTION PERMISSION STATEMENT

*Permission Granted*

# DESIGN AND SIMULATION OF A MEMS LONG DISTANCE TRAVELING MICRO-ACTUATOR

**I, Younes Elkacimi, hereby grant permission to the Wallace Library of the Rochester Institute of Technology to reproduce my thesis in whole or in part. Any reproduction will not be for commercial use or profit.**

**Signature of Author:** _____ **Date:** 08/13/2004

# ACKNOWLEDGMENT

I would like to commence by saying that I have a number of people to thank. First of all I would like to thank my parents, and especially my father may Allah have mercy on his soul, for all the support they have given me, and for being the reason I am here today at this point of my academic career.

I would also like to thank my advisor and mentor for whom I have the highest esteem, Dr. Mustafa Abushagur for his guidance, and assistance with choosing this topic and leading me through it every step of the way. Thank you for giving me the opportunity to pursue something new, and for all the great ideas and thoughts you shared with me. This would not have come to pass if it were not for your support.

As well, I would like to thank Dr. Lynn Fuller who has been of tremendous help to me in completing this work. I have learned a great deal about MEMS and other things too from you over the past couple of years. Dr. Hany Ghoneim has always been of great assistance to me in many ways. You have always seen a great potential in me and I thank you for that. Dr. Alan Raisanen, Dr. Edward Hensel, and Dr. Wayne Walter, I want to thank you for all the assistance you provided me with and for being there to answer any and all the questions I have come to you with.

I would equally like to thank the ME department staff, especially Ms. Connie LaBarre and Ms. Sheila Garwood, and from the dean's office Ms. Mary Jane Frind and Ms. Sharon Stevens.

Last but not least, I would like to thank all my colleagues and friends who directly or in some way helped me with this work.

# ABSTRACT

This thesis is primarily concerned with the design, synthesis, modeling, and simulation of a linear micro-actuator that is able to travel relatively long distances upon the application of a bias voltage. The theoretical investigation addresses the functionality of this device in a certain setting given fixed and variable parameters. The objective of this investigation is to lay out a mathematical model, which explains the physics behind the workings of this device. It is not the objective of this investigation to study all the possible different scenarios that would result by changing certain or all the variable parameters, rather to prove that the concept of a traveling linear micro-actuator is sound. Furthermore, demonstrate that this device is functional to the specifications to which it was designed.

The theoretical analysis was very critical in determining reasonable approximations for the parameters and dimensions of the device used to design the layout, and the process flow necessary for the fabrication process. The detailed explanation of each fabrication step is described in this thesis.

The theoretical analysis shows that this linear micro-actuator, which has a relatively similar function to a parallel comb drive, can operate due to the electrostatic force generated upon the application of a bias voltage. This analysis, also, demonstrates that several other parameters have a direct effect on the performance of the device. Parameters, such as the thickness, the width, and the

length of the electrodes are mathematically proven to change the magnitude of the electrostatic force responsible for the generation of the motion of the moving part of the micro-actuator. This device is comprised of two main components: a conductive fixed support, which works as a fixed electrode, and a moving electrode that would slide over this support and works as a shuttle. It is expected that the shuttle could be used in different applications as a transportation tool for other MEMS components or devices.

# TABLE OF CONTENTS

# List of Figures

# Chapter I - Introduction

## 1.1. Historical Background of MEMS

The term MEMS was coined around 1987, when a series of three workshops on Microdynamics and MEMS was held in July 1987 at Salt Lake City, Utah; in November 1987 at Hyannis, Massachusetts; and in January 1988 at Princeton, New Jersey, leading in a new era of microdevices. The field of solid-state transducers, which has become known as microelectromechanical systems, has traditionally been application driven and technology limited, and has emerged as an interdisciplinary field, which involves many areas of science and engineering. The MEMS industry is expected to follow a similar trend. It is believed that the field of solid-state transducers has been around since the late 1960's. It is generally agreed that the first MEMS device was a gold resonating MOS gate structure [1].

Rotational and linear micromotors are often found to be a key part of micromechanical systems allowing them to perform physical functions. They can be used for aperture or gap controlling, and driving forces for micro-relays, micro-mirrors and micro-grippers amongst other applications. The most commonly used activation principle for micromotors is the electrostatic field between the plates of capacitors including comb drives, curved electrodes, scratch, wobble, linear stepping and side drives with synchronous and asynchronous operation [2].

MEMS today is more precisely defined [3] as the batch-fabricated integrated microsystem (motion, motionless, radiating energy, energy sources, and optical microdevices/microstructures – driving/sensing circuitry –controlling/processing ICs) that:

1. Converts physical stimuli, events, and parameters to electrical, mechanical, and optical signals and vice versa;
2. Performs actuation, sensing, and other functions;
3. Comprises control (intelligence, decision-making, evolutionary learning, adaptation, self-organization, etc.), diagnostics, signal processing, and data acquisition features, and microscale features of electromechanical, electromagnetic, electronic, electrooptical, optical, electrochemical and biological components (structures, devices, and subsystems), architectures, and operating principles are basics of the MEMS synthesis, operation, design, analysis, and fabrication.

MEMS are comprised and built using microscale subsystems, devices, and structures. The batch-fabricated integrated microsystem, can integrate the following components (devices or subsystems):

· motion and/or motionless microdevices/microstructures,
· radiating energy microdevices/microstructures,
· energy sources,
· optical microdevices/microstructures,
· driving/sensing circuitry – controlling/processing ICs).

## 1.2. The Growing Trend of the MEMS Industry

Micro-Electro-Mechanical Systems Technology exploits the existing microelectronics infrastructure to create complex machines with micron feature sizes. These machines can have many functions, including sensing, communication, and actuation. MEMS technology, through micro-fabrication, is the integration of mechanical elements, such as pressure sensors, actuators, stepper motors, and electronics on a silicon substrate. The micromechanical components are fabricated using micromachining processes that selectively etch away parts of the silicon wafer or add new structural layers to form the mechanical and electromechanical devices. The electronics, however, are fabricated using integrated circuit (IC) process sequences such as CMOS (Complementary Metal-Oxide Semiconductor) processes [4]. A critical difference between integrated circuits and MEMS is that ICs are purely electrical devices with no moving parts, while MEMS often contain moving parts such as sensors, actuators, gears, or mirrors. For example, the accelerometers used to trigger car airbags are MEMS devices, as are various micro-flow controllers used in medical applications.

The background of MEMS lies in the solid-state IC technology. After the integrated circuits, the next steps towards MEMS were the development of microfabricated sensors, and the invention of movable micromechanical parts. MEMS have ultimately been intended to become mass-produced with a low unit cost. The concept of micromachine has, in turn, precision engineering and

mechanical background and the idea behind it has been the development of real miniaturized 3-D machines.

MEMS promise to revolutionize nearly every product category by bringing together silicon-based microelectronics with micromachining technology. This merging of technologies makes it possible to realize complete systems-on-a-chip. MEMS is an enabling technology allowing the development of smart products, augmenting the computational ability of microelectronics with the perception and control capabilities of microsensors and microactuators and expanding the space of possible designs and applications [4]. In addition to the microfabrication techniques, micromechanics, microsensors, microactuators and various microsystems, microsystem technology covers design, simulation, integration, control and scaling issues.

## 1.3. MEMS Devices and Applications

There are numerous applications possible for MEMS. MEMS are already used for tasks ranging from in-dwelling blood pressure monitoring to active suspension systems for automobiles. Some of these applications have been realized and are widely used today all over the world. The automobile industry uses pressure and flow sensors, as well as, fuel injectors, and other MEMS devices. Micro-Electro-Mechanical Systems are used in refrigerators, washing machines, microphones, TV screen projection, ink jet printers, smart home controls, boat speedometers, and many other tools and machines.

In biotechnology MEMS technology is enabling new discoveries in science and engineering such as the Polymerase Chain Reaction (PCR) microsystems for DNA amplification and identification, micromachined Scanning Tunneling Microscopes (STMs), biochips for detection of hazardous chemical and biological agents, and microsystems for high-throughput drug screening and selection in a variety of machines and disciplines [4]. Micromechanics is a rich, diverse field that draws on many different disciplines and has other potential applications in military, industrial controls, information apparatus, optics, medicine, electronic interfaces to physical phenomena, consumer products, airplanes, microsatellites, and much more.

The following is a Pressure sensor integrated with CMOS circuitry, developed by CNM (Centro Nacional de Microelectrónica, E) [5]

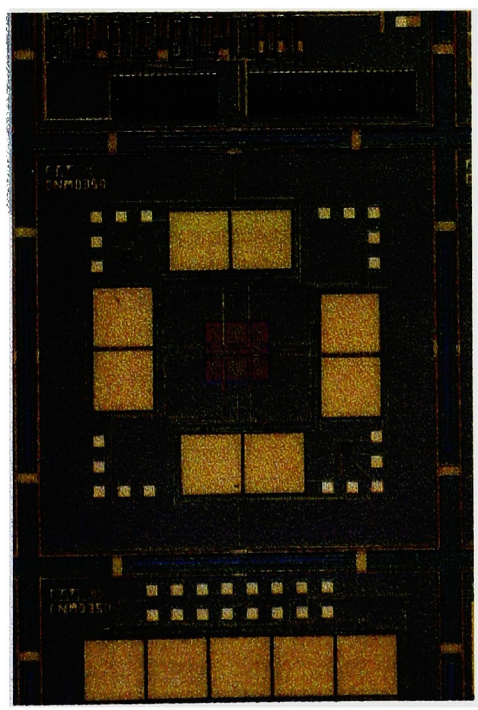

**Figure 1. A Pressure sensor integrated with CMOS circuitry, developed by CNM (Centro Nacional de Microelectrónica, E) [5]**

The following is a six-gear chain, in which all the gears are driven sequentially by the drive-gear (top center). The fixed guide plates (mounted to the tops of the gears' shafts) are clearly visible. Gear chains such as this one have been driven at speeds up to 250,000 RPM.

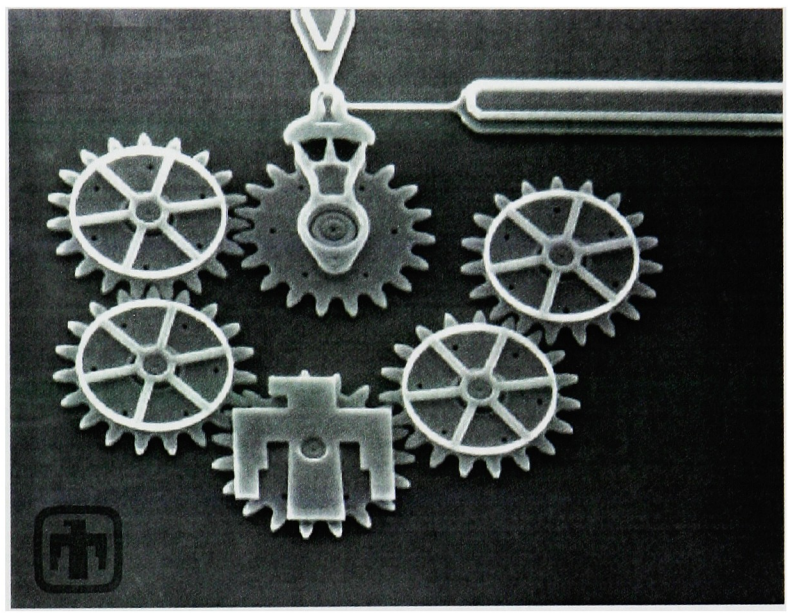

**Figure 2. Six-gear Chain**
**"Courtesy Sandia National Laboratories, SUMMiT™ Technologies, www.mems.sandia.gov"**

## 1.4 Linear Long Distance Traveling Microactuator:

The concept behind the long distance traveling micro-actuator is simple. It is, basically, an actuator operating by virtue of electrostatic force. This micro-actuator device is composed of three main parts. One part constitutes a long conductive fixed track directly attached to a nitride layer, which is deposited on the top of the main surface (Silicon substrate). The other component is the

shuttle, which is a conductive carrier made out of doped polysilicon that slides over the fixed track. This shuttle has lateral poles 'bumps' on both opposing sides parallel to the track. The third part is a set of electrodes built on both sides of the track, in a way that would allow the bumps on the shuttle (in this case 12 poles- six on each side of the shuttle) to completely overlap with some of the fixed electrodes at any given time, and partially overlap with others (refer to Figure 3). This design will allow the shuttle to move (slide) over the track upon the application of a bias voltage.

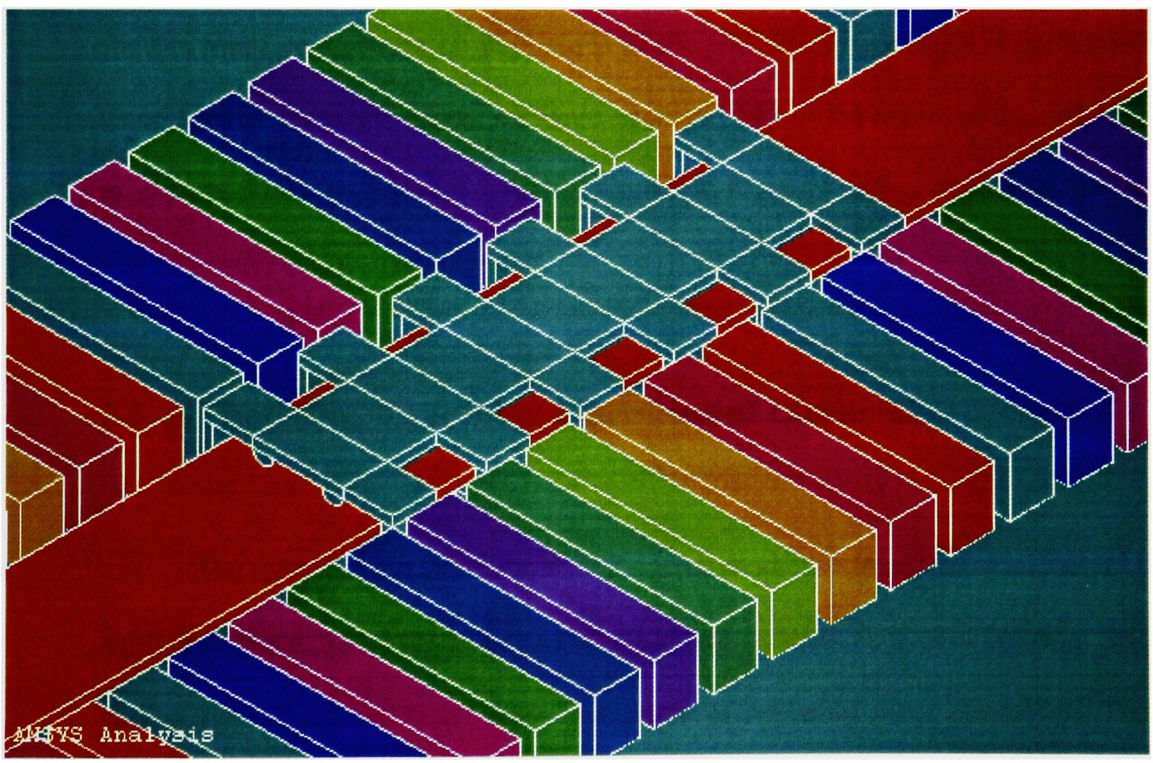


**Figure 3. A solid 3D drawing of the linear microactuator drawn to scale**

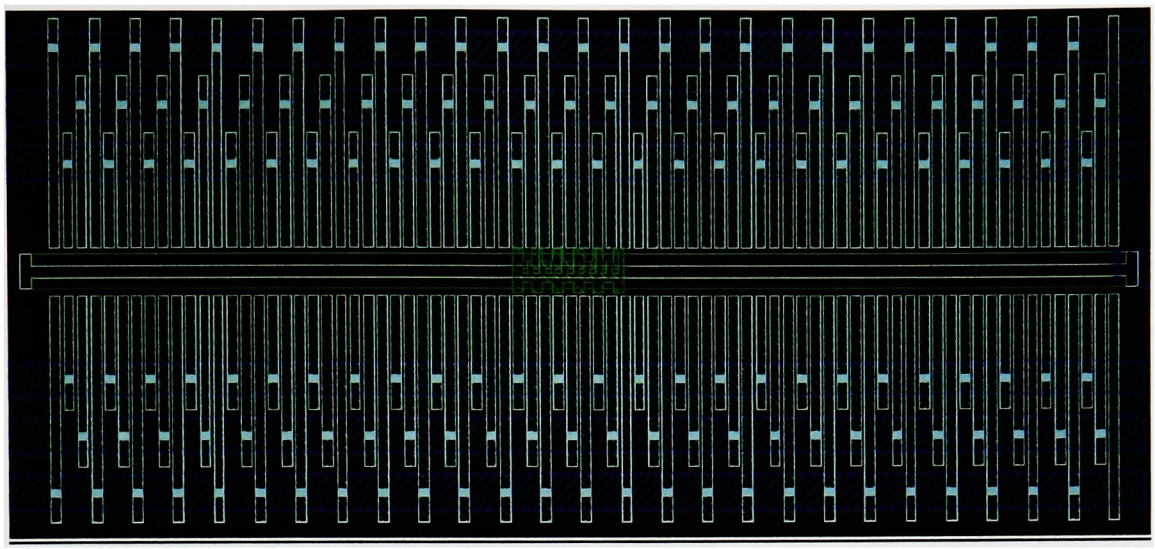

**Figure 4. Mentor Graphic image of part of the device (the track, shuttle, and fixed electrodes) showing all the layers.**

Figure 4 above shows a design layout of a part of the device, which constitutes the shuttle, track, and stators on both sides of the shuttle. This design is performed using Mentor Graphics design software package, and all the layers of the different masks are shown in Figure 5, which is similar to Figure 4 as it is explained further and in greater detail in chapter 4.

## 1.5. A Simplified Concept of Operation of Linear Microactuator

The idea behind the concept of operation of the linear microactuator is similar to that of a synchronous side drive motor (schematic shown below). The sliding anchor (shuttle) is set between two sets of opposing stator electrodes. The stator poles and sliding poles (shuttle poles) are laid out in a fashion, which allows a few of the stator poles to be completely overlapping with other poles on the sliding anchor. The stator poles and the sliding anchor are charged and move the anchor by tangential electrostatical forces as long as the electrode faces

remain shifted. When the faces stand opposite to each other, the next stator electrodes are charged and so on. Sample illustration in Figure 6 below.

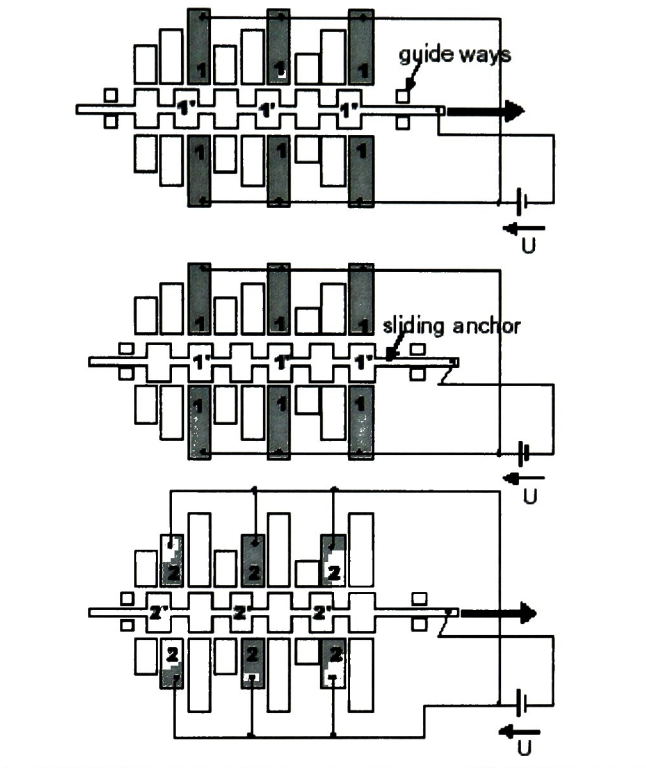


**Figure 6. Synchronous side-drive motor [6].**

## 1.6. Motivation

Electrostatic force is one of the most widely used actuation principles in many different types of micro-actuators. Continuously rotating motors and side-drive motors use this electrostatic force to operate, and so are linear electrostatic motors. Although there have been different types of linear micro-motors studied and built before, the concept we are addressing here in this thesis is a novel one. Many challenges had to be overcome, especially in the design process and

modeling due to the dimensional requirements, which had to be determined and then reviewed and adjusted as the design of the device progressed.

## 1.7. Objectives

The main objectives of this thesis work are to demonstrate analytically and through modeling simulation that the concept of a linear long range (order of a 1000 microns) traveling micro-actuator is sound and applicable. It is also the goal of this experimental study to develop a flow process that is suitable for the manufacturing of such a device using RIT laboratory fabrication capabilities (fabrication of this device, however, is not a part of this thesis). In addition some of the silicon surface micromachining processes that are used during the device fabrication, surface physics, stiction, friction, and phenomenon that would affect the operation and fabrication of the micro-actuator are addressed.

# Chapter II – Theoretical Analysis

## 2.1. Actuation Principles

There are many mechanisms of actuation such as electrostatic, electromagnetic, piezoelectric, and thermal. Each one of these techniques has its advantages and disadvantages. The right choice of the actuation principle is dependent on the structural dimensions, the technology, the response time, the force as a function of displacement, the maximum power consumption, and other factors as well. In this work, an electrostatic-based actuator is selected. Normally, electrostatic-based actuators can move through large displacements, but are only capable of delivering relatively small forces compared to piezoactuators, for instance, which can deliver a large force through very limited displacement [7]. Electrostatic actuation is the most frequently applied principle combining versatility and simple technology. It needs neither additional elements like coils or cores, as it is the case for electromagnetic actuators, nor special materials like shape-memory-alloys or piezoelectric ceramics. Shape Memory Alloys are metals, which exhibit two very unique properties. First is the shape memory effect, which is their ability to be severely deformed and then returned to their original form simply by heating them. Their second property is their pseudo-elasticity, which gives them their almost rubber-like flexibility.

Electrostatic actuation draws its force from the relation of surface-to-surface spacing and not from the relation of volume-to-volume spacing [6]. Micro-actuators can be excited in several ways, including piezoelectric films,

thermal expansion, shape memory alloy actuation, magnetostatic and electrostatic actuation. Because of the simplicity and compatibility with micromachining, such as surface micromachining technology, electrostatic excitation is a very popular approach.

For the intended purpose in this thesis, which is to prove that the concept of such an electrostatically driven linear microactuator is feasible, and both physically and analytically doable, the study of the electrostatic force is important and is the subject of the next section.

## 2.2. Electrostatic Principle

In order to understand how the proposed electrostatically driven microactuator would work, synthesis, design, and modeling, and understanding of the electrostatic force in flat conductive plates (capacitors), comb drives, and other electrostatic actuators and micromotors is important. This approach was chosen, because it facilitates the understanding of the operation mechanism of the linear microactuator in question.

### 2.2.1. Electrostatic Field Lines

The presence of an electric charge produces a force on all other charges present. The electric force produces action-at-a-distance; the charged objects can influence each other without touching. Suppose two charges, $q_1$ and $q_2$, are initially at rest. Coulomb's law allows us to calculate the force exerted by charge $q_2$ on charge $q_1$ (see Figure 7). At some point in time charge $q_2$ is moved closer to

charge $q_1$. As a result we expect an increase of the force exerted by $q_2$ on $q_1$. However, this change cannot occur instantaneously (no signal can propagate faster than the speed of light). The charges exert a force on one another by means of disturbances that they generate in the space surrounding them. These disturbances are called electric fields. Each electrically charged object generates an electric field, which permeates the space around it, and exerts pushes or pulls whenever it comes in contact with other charged objects. The electric field E generated by a set of charges can be measured by putting a point charge q at a given position. The test charge will feel an electric force F. The electric field at the location of the point charge is defined as the force F divided by the charge q.

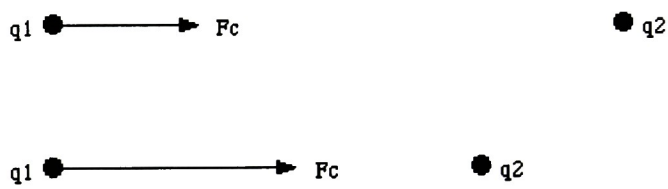


**Figure 7. Electric force between two electric charges.**

$$\vec{E} = \frac{\vec{F}}{q}$$

The definition of the electric field shows that the electric field is a vector field: the electric field at each point has a magnitude and a direction. The direction of the

electric field is the direction in which a positive charge placed at that position moves [8].

### 2.2.2. Electrostatic Comb Drives and Micro-actuators

An electrostatic comb drive is one of the most important components in MEMS. A standard comb drive is formed by two sets of fingers with uniform gaps. One set is fixed on the substrate, which is called a fixed, or stationary finger. The other set is separate from the substrate and is called a moving finger. Moving fingers can move either laterally with the gaps fixed or vertically with the gaps closing to one side or the other.

Normally the laterally moving comb drive works as an electrostatic actuator. In this way, it can give a constant force and has a large stroke distance. Gap-closing combs often work as capacitive sensors [9].

Comb Drives are particularly popular with surface micromachined devices. They consist of many interdigitated fingers. When a voltage is applied an attractive force is developed between the fingers, which move together. The increase in capacitance is proportional to the number of fingers; so to generate large forces, large numbers of fingers are required. One potential problem with this device is that if the lateral gaps between the fingers are not the same on both sides, then it is possible for the fingers to move at right angles to the intended direction of motion and stick together until the voltage is switched off.

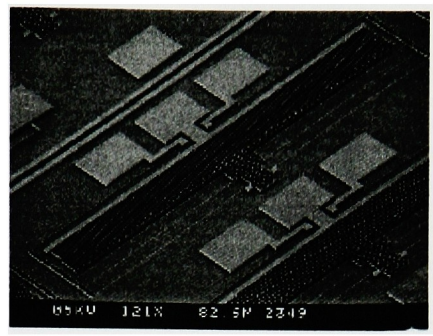

**Figure 8. SEM photo of comb drive actuators [10]**

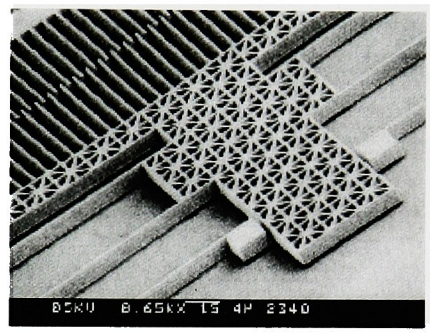

**Figure 9. Close up of the shuttle [10]**

Capacitance between two flat plates each of area A, length l, and, height h, is defined [9]:

$$C = \varepsilon_0 \varepsilon_r A/d \qquad (1)$$

where,

d = the separation gap

$\varepsilon_0 = 8.854 \times 10^{-12} F/m$ is the dielectric constant of free space

$\varepsilon_r$ = Dielectric permittivity (equals 1 for air)

Change in capacitance when moving by a distance Δl

$$\Delta C = \varepsilon_0 \times \varepsilon_r \times \Delta A / d \tag{2}$$

$$\Delta C = \varepsilon_0 \times \varepsilon_r \times (\Delta l \times h) / d \tag{3}$$

Electrostatic Forces: Parallel Plate Capacitor: Both plates are fixed

The following is the expression for the electrostatic force of a capacitor with two flat plates [9]. V is the bias voltage applied, and d represents the distance between the two plates. C is the capacitance.

$$F = \frac{1}{2} \times \left( \frac{C}{d} \right) \times V^2 \tag{4}$$

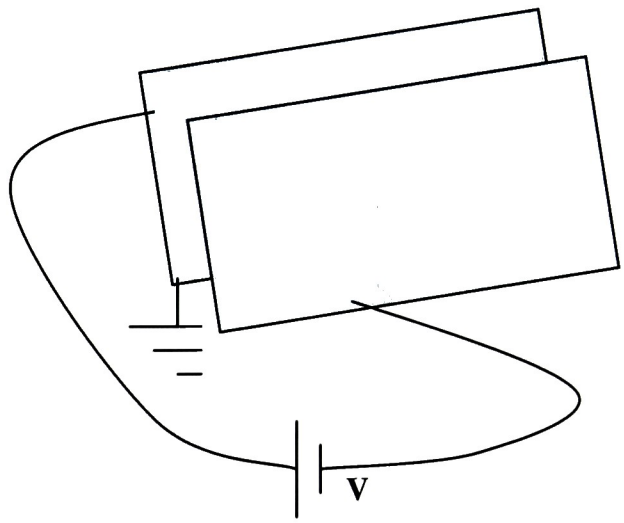


**Figure 10. Schematic of a parallel plate capacitor**

### 2.2.3. Electrostatic Actuation

Example of linear Comb Drive: (Electrostatic micro-actuator)

The following section discussing a sample of an electrostatic comb-drive actuator is based in part on a work published by P. Rai-Choudhury [7], and Yongjun Zhao in [9]

An actuator is defined as an element that applies a force to an object through a distance. It performs work as it moves from point a to point b.

$$W = \int_a^b F dx \tag{5}$$

where F is the force vector and x is the displacement vector

The gap-closing force is one of two forces acting during the operation of a linear microactuator. A parallel-plate electrostatic capacitor with two plates in which one plate is fixed and the other one is moveable, as shown below, has an electrostatic force expressed as follows:

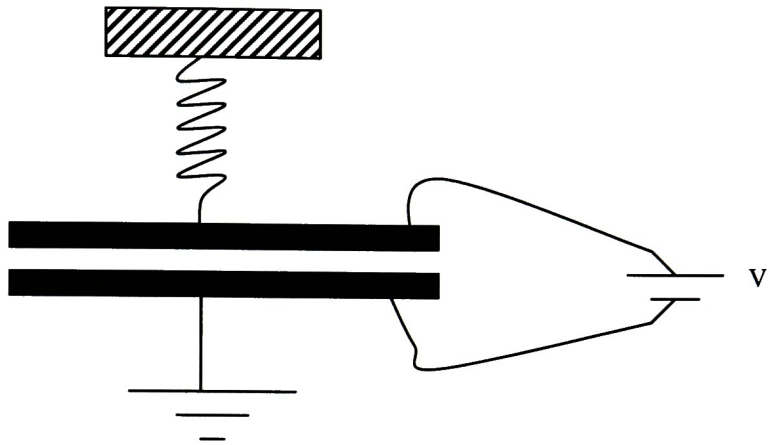


**Figure 11. Schematic of a parallel Plate Capacitor with One Fixed Plate**

Positioning of capacitor plate:

$$F = \left(\frac{1}{2} \times \frac{\varepsilon_0 \varepsilon_r A}{d^2}\right) \times V^2 \qquad (6)$$

where each plate has an area A, d is the separation gap, and V represents the constant potential applied. To get an idea of the magnitude of the electrostatic force generated in such flat plate capacitor we consider the following numerical application. For actuators with plates 50x50 $\mu m^2$ and the gap d=2 $\mu m$, the force obtained is 2.5 $\mu N$ at potential V=30 volts.

The higher the voltage (V), the closer the plate is pulled in, and the electrostatic force F goes to infinity when d tends towards 0.

The electrostatic force for parallel-plate (gap-closing force) electrostatic capacitor can also be expressed as:

$$F = \left(\frac{1}{2} \times \frac{n\varepsilon hx}{g^2}\right) \times V^2 \qquad (7)$$

where: F: electrostatic force caused by applying a voltage between the two electrodes

ε: diaelectric constant of free space

g: gap between the two electrodes (in this case it is constant)

h: thickness of the electrodes

x: overlapping distance (changes; it is the variable in the equation above)

n: the number of fingers or poles

Usually all the parameters are assumed constant, except for the overlapping distance, which changes with time.

The force of a parallel plate capacitor varies as $\left(\frac{1}{d^2}\right)$, or $\left(\frac{1}{g^2}\right)$. It is a nonlinear force under constant bias voltage.

Lateral Electrostatic force:

In a comb-drive electrostatic actuator as the one shown in the schematic below, when a voltage V is applied,

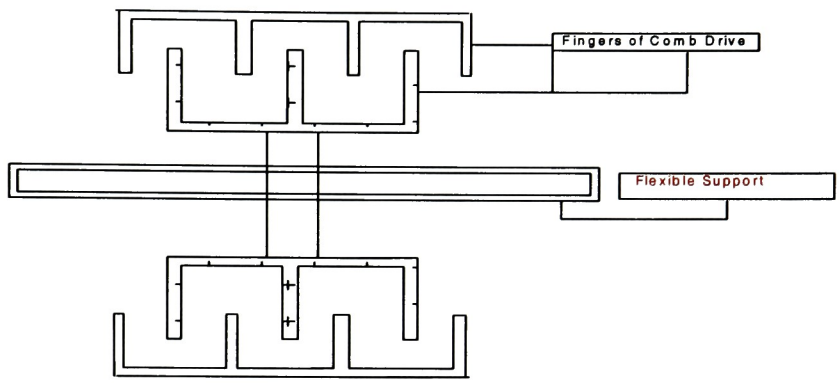


**Figure 12. Comb Drive Electrostatic Actuator**

an attractive force developed between the fingers moves the suspended part. The increase in capacitance is proportional to the number of fingers or poles. The electrostatic force in this case is expressed as follows:

$$F_{el} = n\varepsilon_0\varepsilon_r\left(\frac{h}{d}\right)V^2 \qquad (8)$$

where n is the number of fingers in each electrode, h is the height of fingers (electrode), and d is the overlapping distance of the fingertips between the two electrodes.

One of the most important features of a lateral comb drive is that a constant driving force with a large stroke distance can be obtained under constant

bias voltage. This linear relationship gives many benefits to design varieties of micro sensors or actuators similar to the proposed design for this thesis.

The force of a comb drive, as was mentioned earlier is generally constant for any value of the gap, but when the moving fingers strike close to the support beam of the fixed fingers, this constant force feature is no longer sustained. Now the capacitance between the cross section of the moving finger and inside wall of the support beam of the fixed finger is significant.

Because the gap distance is normally smaller relative to the height and overlap length, a gap-closing driven comb drive has a larger force than a laterally- driven comb-drive.

### 2.2.4. Design Specifications [11]

- In a comb drive, the thickness (height) t is typically limited to about 2 to 3 micromiters in surface micromachining technology.
- Typical gap width is about one micrometer

## 2.3. Mathematical Model

In many important microelectromechanical systems (MEMS) applications, such as micro grippers, comb drives, and micro-mirrors, electrostatic actuation is favored over other more complex or higher power options such as thermal, magnetic or shape memory processes. The modeling of electrostatic actuator systems has attracted considerable attention in the literature for a wide variety of actuator types. These include actuators with various electrode shapes and sizes,

and designs that employ the use of series capacitors, and residual stresses. Usually the models take a force-based approach to calculate the static device behavior by considering the balance between the attractive electrical force and any elastic restoring forces. This approach typically leads to a structural equation that predicts the actuator position as a function of applied voltage, and defines the stable, low voltage region of operation prior to runaway or pull-in, where the nonlinear electrostatic force overcomes the typically linear restoring force, or the forces impeding the motion [12].

For the laterally driven linear microactuator being studied in this case, a model of the device was created, in which all the external forces that have a noticeable effect were determined and included to develop an equation of motion for the microsystem. The differential equation was then solved and results for the displacement, velocity, and force as a function of time, friction, and voltage applied have been obtained. This microactuator differs from other similar devices in its design structure.

### 2.3.1. Mechanical System

The main body of the proposed laterally driven electrostatic microactuator can be modeled as a classical second order mechanical system with a single degree-of-freedom.

According to Newton's second law, the differential equation of motion of a forced second order mechanical system is given by:

$$m \cdot x'' = \sum_{n} F \tag{9}$$

where m is the mass of the shuttle (the moving electrode), x its displacement along the track (fixed electrode), and F representing the external forces the shuttle is being subjected to.

In MEMS devices, various forces associated with the devices scale down with the size. When the length of the machine decreases from 1 millimeter to 1 micron, the area decreases by a factor of a million and the volume decreases by a factor of a billion. The resistive forces such as friction, viscous drag and surface tension that are proportional to the area increase a thousand times more than the forces proportional to the volume such as inertial and electromagnetic forces [13].

As it was stated earlier, this device is electrostatically driven, therefore the force responsible for the motion of the shuttle is the electrostatic force $F_e$ generated due to the application of a bias voltage. The shuttle, being the moving part in this microsystem, is situated on the top of, and therefore touching, the fixed track by means of 'dimples' (refer to cross sectional area schematic, Figure 13) below. These dimples were designed to minimize surface friction between the shuttle and its support (more on this subject later).

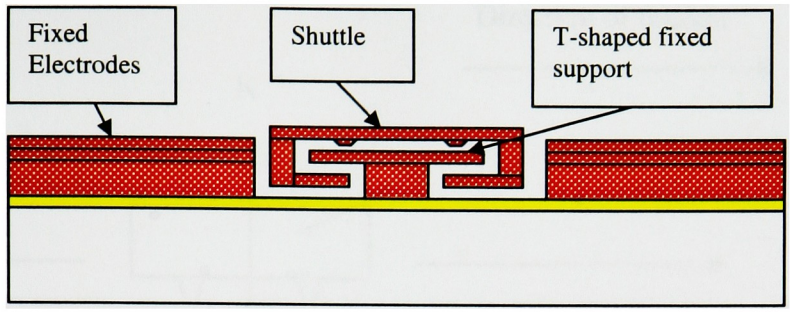


**Figure 13. Schematic of the Cross sectional Area of the linear Actuator**

This contact of the shuttle and the T-shaped support is cause for dry friction force (or coulomb force) $F_C$, which will work to impede the motion of the transport. Since this device is designed to operate in air under normal room temperature and atmospheric conditions, the drag force $F_D$ is, thus, another external force the shuttle is being subjected to. The latter serves to slow down the motion of the moving component once the device is set in motion.

Now the equation of motion (9) becomes:

$$\Rightarrow \quad m \cdot x'' = F_e - F_D - F_C \tag{10}$$

$$\Rightarrow \quad m \cdot x'' + F_D = F_e - F_C \tag{11}$$

A free body diagram to illustrate the forces the shuttle is subjected to follows:

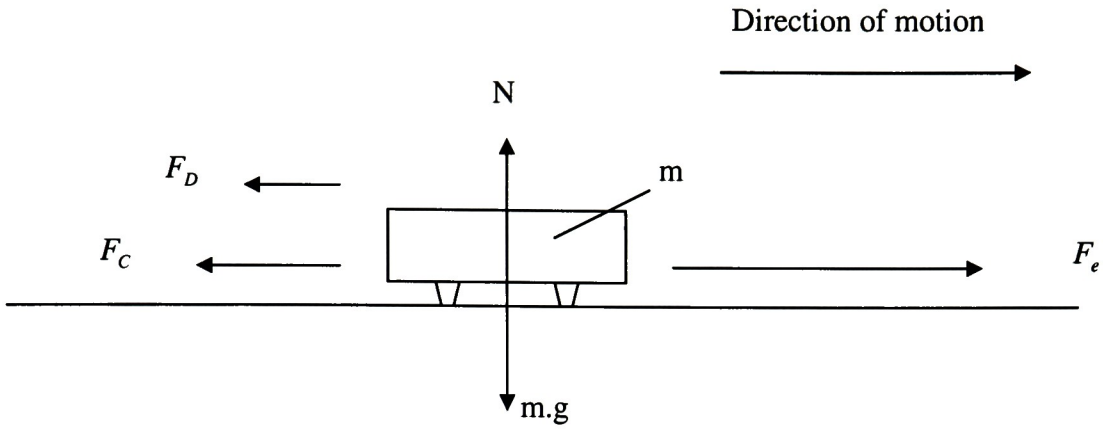


**Figure 14. Schematic Diagram of the External Forces Exerted on the Shuttle**

### 2.3.2. Electrostatic Forces

The microsystem being studied here is a shuttle in motion. This vehicle moves due to electrostatic force, which is generated upon the application of a bias voltage. This voltage is applied between the fixed electrodes, on both sides of the shuttle simultaneously using a three-phase generator, and the shuttle (moving electrode). Both the poles on the shuttle and the fixed electrodes on both sides of the shuttle have rectangular shapes, and are designed to have their respective cross-sectional areas facing each other in order to maximize the electrostatic force generated between them (refer to Figure 13 above).

The device was designed to have a gap of 2 microns between the poles of the shuttle and the fixed electrodes. It was mentioned earlier that the two types of electrostatic force are at work here. The gap-closing force is working to get the two surfaces (considering, for simplicity, one set of poles—one moving pole on the shuttle and the other one fixed) closer together. The expression for this force

as we discussed earlier is: $F = \left(\frac{1}{2} \times \frac{n\varepsilon hx}{g^2}\right) \times V^2$. This force is of no interest in this case, because the vehicle was designed in a way that will not allow it to move sideways of the track it is sliding on. In other words, when the same bias voltage is applied to the fixed electrodes on both sides of the shuttle and the shuttle itself, the electrostatic force generated on both sides of the shuttle has the same magnitude and direction, which serves to stabilize the shuttle and prevent it from tilting to either side of the track. Moreover, the shuttle is built on a T-shaped track, which is supposed to carry the shuttle, supply voltage to it, and reduce its motion to the right and left of the track.

Now, the only part of the electrostatic force to be considered in this case is the lateral force. This force, as was shown previously, has the expression: $F_{el} = \frac{1}{2} n \varepsilon_0 \varepsilon_r \left(\frac{h}{d}\right) V^2$. It is a function of the number of poles on the shuttle, their height, the gap between the poles on the shuttle and the poles on the fixed electrodes, and the voltage. The direction of this force is that of the motion of the vehicle.

### 2.3.3. Fringing Fields

At the edges of the plates of a parallel-plate capacitor, in general, there is 'fringing' (edging) of the electrostatic field. The charge can appear at the outer edges of the plates. In this model, the influence of fringing field is neglected, which is a reasonable approximation for the investigated microactuator, as finite-element calculations [14] revealed maximum contributions to the electrostatic force (Fe) of less than 10% for capacitor plate overlaps of 10 microns or greater

(The width of the stators or poles of the microactuator being studied in this thesis is 10 microns).

Also, It was shown in previous research [15] done with micromotors with similar dimensions, principle of operation, and operating conditions that the effects of the fringe fields on the output response are negligible.

### 2.3.4. Drag and Lift Forces

The following discussion in this segment about drag friction is based on the work published by Mohd P. Omar, Merhan Mehregany, and Robert L. Mullen in [16] and by Robert L. Mott in [17].

A moving body immersed in a fluid experiences forces caused by the action of the fluid. The total effect of these fluids is quite complex. However, for the purpose of design or for the analysis of the behavior of a body in a fluid, two resultant forces (drag and lift) are the most important. Lift and drag forces are the same regardless of whether the body is moving in the fluid or the fluid is moving over the body.

Lift is a force caused by the fluid in a direction perpendicular to the direction of travel of the body. The magnitude of the lift must at least equal the weight of the device in order for it to fly. For most practical aerodynamic shapes, the lift is generated mainly by the surface pressure distribution; the shear stress distribution generally makes only a small contribution [18].

While there has been considerable work on MEMS scale airflows in internal flow geometries, such as microchannels, there are few experimental results of external-

flow configurations, such as the one being studied in this thesis. Previous research [19] details an experimental study planned for flat plate airfoils at the MEMS scales. This experimental work entailed the creation of an integrated micro-airfoil/micro-force sensor in order to be able to measure drag and lift on a microscale airfoil with dimensions similar to those of the shuttle being studied in this case (order of 10 to 100 microns). Theoretical and numerical results suggest the decrease in drag due to non-equilibrium effects should be measurable on flat-plate airfoils, with a chord of 10 to 100 microns, at pressures ranging from 0.1 to 1.0 atmospheres, and velocities from 30 to 100 m/s. These are similar conditions to the ones the electrostatically driven microactuator is supposed to be operating at. These conditions are a shuttle length of 100 microns, span (width) less than 10,000 microns, atmospheric pressure of 1 atmosphere, and velocities in the order of 10 m/s as it is discussed in the Results Analysis section below.

Currently, there is no flow visualization technique suitable for studying the structure of a MEMS scale boundary layer [19]. However, this experiment basically concluded that slip at the surface will reduce the skin friction at the wall. On a microscale airfoil, this will result in a decrease in drag. The effect on lift is not well understood.

It is then obvious that at the microscale level, lift of airfoils, such as the shuttle being considered cannot be studied using classical Newtonian Mechanics without some modifications, since the physics and the behavior of boundary layers is different and not very well understood at the microscopic level.

Moreover, in this case of the shuttle traveling on a fixed horizontal track, lift is not an issue because the shuttle will always remain flat on the track and parallel to the direction of the thrust, which is the electrostatic force responsible for moving the device.

To illustrate this let's look at the following free body diagram:

Assuming steady level translation motion of the shuttle on the track (no acceleration). The angles are exaggerated for illustration purpose and better visibility.

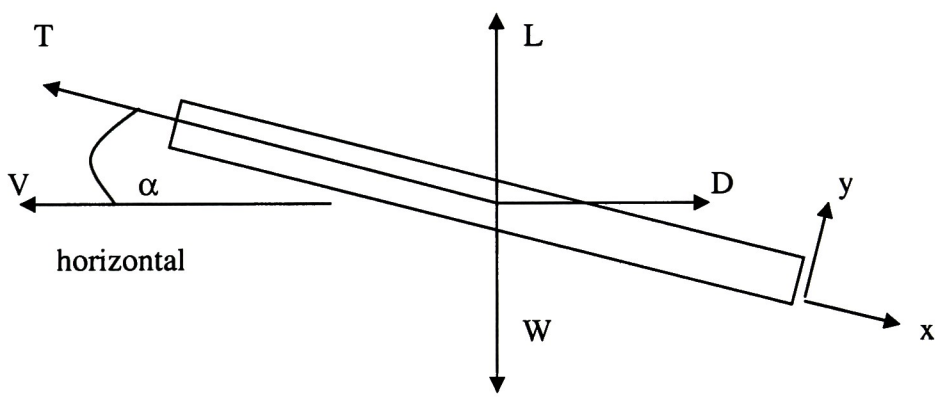


**Figure 15. FBD of a Flat Airfoil (Shuttle)**

T is the thrust provided to move the (airfoil) shuttle (represented in this simplified F.B.D. by the rectangle), D is the drag force, L is the lift, W is the weight of the airfoil, V is the velocity, and $\alpha$ is the "angle of attack" between the thrust vector (chord line) and the horizontal (free stream) [20]. The lift L and the drag D vary with this angle [21].

Lift: $L = W - T * \sin(\alpha)$ (12)

Drag: $D = T * \cos(\alpha)$ (13)

However, the angle of attack in the case considered in this thesis is zero, because the shuttle is always parallel to the direction of the translation motion. Which explains why there is no lift involved in this case.

Even in the case where there is acceleration and thus, unsteady level motion, the lift would still be of no effect to the motion of the airfoil (shuttle).

Furthermore, since the shuttle is designed in a way that would prevent it from leaving its track (flying) (refer to cross-sectional schematic of the shuttle – Figure 13), and knowing that even when the lift takes place the shuttle can only move up a distance of less than 2 microns (the gap between the shuttle and the fixed track), the lift is not, therefore, significant and would not be considered in any further analysis of the motion of the vehicle.

Drag is the force on a body caused by the fluid, which resists motion in the direction of travel of the body. The drag force must be opposed by a propulsive force in the opposite direction to maintain or increase the velocity of the vehicle (micro-device, which is the shuttle in this case). Since the production of the propulsive force requires added power, it is desirable to minimize drag.

The drag force is usually expressed in the form:

$$F_D = \frac{1}{2} C_D \cdot \rho \cdot A \cdot (x')^2 \qquad (14)$$

- $C_D$ is the drag coefficient. It is a dimensionless number that depends on the shape of the body and its orientation relative to the fluid stream.
- $\rho$ is the density of the fluid (air in this case)

- v (or $\dot{x}$) is the velocity of the free stream of the fluid relative to the body. In general it does not matter if the body is moving or if the fluid is moving.
- A is some characteristic area of the body. Most often the area of interest is the maximum cross sectional area of the body, sometimes called the projected area. This is the area used to compute the drag on a vehicle, called the 'form drag' or the 'pressure drag'. But for relatively long, smooth shapes, such as the shuttle in the device being studied, the surface area is used. In this case the 'friction drag' as the air flows along the surface of the vehicle is of concern.
- The combined term $\frac{1}{2}\rho v^2$, is called the dynamic pressure, which the drag force is proportional to. Since, the dynamic pressure is proportional to the velocity squared, then, doubling the velocity for the moving vehicle will increase the drag force by a factor of four.

### 2.3.5. Friction Forces

Studies have been conducted to measure the friction/stiction in micromotors, turbines and gear structures, and polysilicon microstructures to understand friction mechanisms. S. Sundararajan and B. Bhushan from Ohio State [13] conducted studies on four different samples and measured surface roughness, and microscale friction, amongst other things, of doped and undoped polysilicon films, undoped single crystal silicon (100), and cubic Sic films (3C-SiC).

Their results show that, as deposited doped polysilicon shows relatively high friction (0.07), which is due to the presence of grain boundaries and high surface roughness. But polishing of the doped polysilicon film results in very low coefficient of friction (0.02).

The same authors collected data on static friction coefficients of various MEMS devices evaluated by various researchers [22]. The techniques used to determine the friction forces employed indirect methods or involved fabrication of complex structures. The atomic force/friction force microscope (AFM/FFM), an ideal instrument for direct measurements of surface phenomenon on MEMS devices, components, and their surfaces, was used to measure these coefficients. The static friction force (stiction) encountered in surface micromachined polysilicon electrostatic micromotors was measured using AFM. These electrostatic micromotors, although having a rotational motion instead of linear motion, resemble the linear electrostatic motor being studied in this essay. The material used is doped polysilicon, the principle force used to operate the device is electrostatic, the bearings are the same, polysilicon on polysilicon surfaces on both types of devices, the polysilicon layer thickness are very comparable, and the voltages used to operate the devices are very comparable as well, as it will be explained further in subsequent sections. The published data on coefficient of static friction measurements of MEMS devices and structures show that for an electrostatic comb-drive using polysilicon on polysilicon material pairs (similar to the material pairs of the device being studied in this thesis), operating in air, the coefficient of static friction is $4.9 \pm 1.0$ [22].

Static frictional forces from the interlocking of the irregularities of two surfaces will increase to prevent any relative motion up until some limit where motion occurs. It is that threshold of motion, which is characterized by the coefficient of static friction. The coefficient of static friction is typically larger than the coefficient of kinetic friction. The coefficient of static friction depends on the character of the two surfaces—the material they are made of, their cleanliness, their degree of polish, and so forth, and it has to be determined experimentally. The coefficient of kinetic friction, also, depends on the character of the surfaces and needs to be measured for use in any practical application [23]. Once motion starts, frictional resistance generally decreases, and thus the kinetic friction coefficient is less than the static friction coefficient. Therefore, the kinetic friction coefficient values that are going to be used in the modeling of this microsystem being studied are going to range between the best case scenario value of 0.07 reported in [13] and the worst case scenario value of less than 4.9 $\pm 1.0$ reported in [22]. Kinetic friction is approximately proportional to the magnitude of the normal force between two sliding surfaces, and it is obtained by multiplying the kinetic friction coefficient and the normal force.

$$F_C = \mu_k \times N \tag{15}$$

$$F_C = \mu_k \times m \cdot G \cdot \mathrm{sgn}(\dot{x}) \tag{16}$$

Where $\mu_k$ is the kinetic friction coefficient, G is the gravitational constant, and m the mass of the vehicle. This last term, which is nonlinear: $\text{sgn}(\dot{x}) = +1$ if the direction is positive, and $-1$ if the direction is negative.

### 2.3.6. Electromagnetic Forces

In MEMS devices, the various forces associated with the devices scale with the size. When the length (dimension) of a MEMS device decreases so does its surface area and volume. But the device's surface area to volume ratio increases dramatically. As a result, the magnitudes of the surface forces such as friction and viscous drag, which are proportional to the surface area, become larger. On the other hand, the magnitudes of the forces, which are proportional to volume, such as electromagnetic forces become much smaller in comparison [22]. Therefore, in the modeling of this statically driven linear microactuator, the electromagnetic forces and their effects have been ignored.

### 2.3.7. Other Forces

There are different forces, which affect the shuttle motion in different ways. One of these forces is stiction (surface static friction), which has been studied extensively in tribology (The science of the mechanisms of friction, lubrication and wear of interacting surfaces that are in relative motion) of magnetic storage systems. Limited studies have also been conducted to address stiction issues in surface micromachining of MEMS. In MEMS devices involving parts in relative motion to each other, such as micromotors, large friction forces

become the limiting factor to the successful operation and reliability of the device [22].

The van der Waals forces are another type of forces, which influences the shuttle motion. These forces are the weakest among all the forces, but they are important because they are always present. The van der Waals forces are short range in nature but, in cases where large molecules or surfaces are involved, they can produce an effect longer than a distance of about 0 to 0.1 $\mu m$.

In MEMS, the van der Waals forces can have significant effects in structures with large surface-to-volume ratios (e.g. The linear electrostatic microactuator being studied, and large-and-thin comb-drive structures) whenever they are in contact with another surface. Stiction or adhesion of the structure to the substrate can often be observed as a major problem in the operation of these structures. Nevertheless, the van der Waals forces between two contacting surfaces are in many cases hard to be separately distinguished from electrostatic (coulombic) forces, which have already been discussed [24].

### 2.3.8. Equation of Motion and Solution to the Representative Differential Equation

The equation of motion (9) we mentioned earlier is

$$m \cdot x'' + F_D = F_e - F_C \qquad (17)$$

where,

$$F_D = \frac{1}{2} C_D \cdot \rho \cdot A \cdot (x')^2 \tag{18}$$

$$F_C = \mu_k \cdot m \cdot G \cdot \mathrm{sgn}(x') \tag{19}$$

$$F_e = \frac{n}{2} \cdot \varepsilon_0 \cdot \varepsilon_r \cdot \frac{h}{d} \cdot V^2 \tag{20}$$

The equation (9) after substitution becomes:

$$m \cdot x'' + \frac{1}{2} C_D \cdot \rho \cdot A \cdot (x')^2 = \frac{n}{2} \cdot \varepsilon_0 \cdot \varepsilon_r \cdot \frac{h}{d} \cdot V^2 - \mu_k \cdot m \cdot G \cdot \mathrm{sgn}(x') \tag{21}$$

The direction of motion chosen is positive (refer to Figure 14 above). Thus $\mathrm{sgn}(\dot{x}) = +1$. equation (21) now becomes:

$$m \cdot x'' + \frac{1}{2} C_D \cdot \rho \cdot A \cdot (x')^2 = \frac{n}{2} \cdot \varepsilon_0 \cdot \varepsilon_r \cdot \frac{h}{d} \cdot V^2 - \mu_k \cdot m \cdot G \tag{22}$$

This is a nonlinear differential equation of the second order. All the parameters in the above differential equation, which are known and constant are simplified. Therefore, for ease, the equation is simplified and becomes:

$$m \cdot x'' + P \cdot (x')^2 = D \tag{23}$$

where,

$$P = \frac{1}{2} C_D \cdot \rho \cdot A \qquad \text{and,} \tag{24}$$

$$D = F_e - F_C \tag{25}$$

$$D = \frac{n}{2}\cdot\varepsilon_0\cdot\varepsilon_r\cdot\frac{h}{d}\cdot V^2 - \mu_k\cdot m\cdot G \tag{26}$$

(22) $\Rightarrow$

$$m\cdot x'' = D - P\cdot(x')^2 \tag{27}$$

$\Rightarrow$

$$m\cdot\frac{d}{dt}x' = D - P\cdot(x')^2 \tag{28}$$

$\Rightarrow$

$$\frac{dx'}{\left[D - P\cdot(x')^2\right]} = \frac{1}{m}\cdot dt \tag{29}$$

Using partial fractions, the expression above is developed to get:

$$\frac{\left(\frac{1}{2\cdot\sqrt{D}}\right)}{\sqrt{D}-\sqrt{P}\cdot x'}\cdot dx' + \frac{\left(\frac{1}{2\cdot\sqrt{D}}\right)}{\sqrt{D}+\sqrt{P}\cdot x'}\cdot dx' = \frac{1}{m}\cdot dt \tag{30}$$

The new developed expression is then integrated to derive an expression for the velocity:

$$x' = \frac{\sqrt{D}}{\sqrt{P}}\cdot\frac{\left[\frac{1}{C^q}\cdot e^{\left(\frac{t}{m\cdot q}\right)} - 1\right]}{\left[\frac{1}{C^q}\cdot e^{\left(\frac{t}{m\cdot q}\right)} + 1\right]} \tag{31}$$

where, t is time, and the constants C and q are defined as follows:

$$C = e^{\left[c_3 - \frac{(c_1 + c_2)}{2\cdot\sqrt{D}}\right]} \tag{32}$$

$$q = \frac{1}{2\cdot\sqrt{P\cdot D}} \tag{33}$$

where, $c_1, c_2, and c_3$ are the constants of integration.

To simplify the expression for the velocity even more, two new constants are defined:

$$C' = C^{\frac{1}{q}} \tag{34}$$

$$\theta = \frac{1}{m\cdot q} \tag{35}$$

Thus equation (31) becomes: (36)

$$\boxed{x' = \frac{\sqrt{D}}{\sqrt{P}}\cdot\frac{\left(C'\cdot e^{\theta\cdot t} - 1\right)}{\left(C'\cdot e^{\theta\cdot t} + 1\right)}}$$

This expression for the velocity of the vehicle is then integrated to obtain equation 37, which is an expression for the displacement:

(37)

$$\boxed{x = \frac{2\cdot\sqrt{D}}{\theta\cdot\sqrt{P}}\cdot\ln\left(\sqrt{P} + \sqrt{P}\cdot C'\cdot e^{\theta\cdot t}\right) - \frac{\sqrt{D}}{\sqrt{P}}\cdot(t)}$$

Using boundary conditions, the constant $C'$ is determined.

$$C' = \frac{1-\sqrt{P}}{\sqrt{P}} \tag{38}$$

Thus, the expression for the displacement becomes as follows:

$$x(t) = \frac{m}{P}\cdot\ln\left[\sqrt{P} + \left(1-\sqrt{P}\right)\cdot e^{\theta\cdot t}\right] - \frac{\sqrt{D}}{\sqrt{P}}\cdot(t) \tag{39}$$

$$\theta = \frac{1}{m\cdot q} = 2\cdot\frac{\sqrt{P\cdot D}}{m} \tag{40}$$

$$\boxed{x(t) = \frac{m}{P}\cdot\ln\left[\sqrt{P} + \left(1-\sqrt{P}\right)\cdot e^{\left(2\cdot\frac{\sqrt{P\cdot D}}{m}\right)\cdot t}\right] - \frac{\sqrt{D}}{\sqrt{P}}\cdot(t)} \tag{41}$$

The expression for the velocity becomes:

$$x' = \sqrt{\frac{D}{P}}\cdot\frac{\left[\left(1-\sqrt{P}\right)\cdot e^{\theta\cdot t} - \sqrt{P}\right]}{\left[\left(1-\sqrt{P}\right)\cdot e^{\theta\cdot t} + \sqrt{P}\right]} \tag{42}$$

Equation 42 becomes equation 43 when the expression for theta is substituted:

(43)

$$\Rightarrow \quad x' = \sqrt{\frac{D}{P}} \cdot \frac{\left[\left(1-\sqrt{P}\right)\cdot e^{\left(2\cdot\frac{\sqrt{P\cdot D}}{m}\right)\cdot t} - \sqrt{P}\right]}{\left[\left(1-\sqrt{P}\right)\cdot e^{\left(2\cdot\frac{\sqrt{P\cdot D}}{m}\right)\cdot t} + \sqrt{P}\right]}$$

The following are the numerical values obtained for the different parameters used in the evaluation of the solution to the differential equation solved above:

N: number of poles on the shuttle = 12 (only six poles in each phase)

$\varepsilon$: air permittivity = $\varepsilon_0 = 8.854 \times 10^{-12} F/m$

h: Electrodes height = 10 microns

g: gap between moving and fixed poles = 2 microns

V: voltage applied ranges from 0 volts to 30 volts

$\mu_k$: Kinetic coefficient of friction ranges from 0.07 to 5.0

m: the mass of the shuttle = $1.99044x10^{-11} Kg$

G: gravitational constant = $9.83 m/s^2$

$C_D$: drag coefficient = 1.1825

$\rho_{Air} = 1.184 Kg/m^3$ = density of air

A: surface area of the shuttle considered for surface friction

$A = 2.7270x10^{-9} m^2$

The above numerical values were used to evaluate the different expressions for all the external forces acting on the device, as well as the displacement and velocity. The numerical results were then substituted into the equations, which were used in turn to plot the different graphs of displacement, motion, and the different motion impeding forces, such as friction and drag. Theses graphs are plotted to help the analyst understand the behavior of the moving shuttle on the track as different values for the kinetic coefficient of friction and voltage are applied.

# Chapter III - Discussion and Analysis:

## 3.1. Results discussion and Analysis

Figure 16 shows the displacement as a function of time using the highest value for the kinetic coefficient of friction and the voltage in the range provided. The kinetic friction coefficient ranges from 0.07 to 5.00 (refer to the above discussion on friction forces), and the voltage ranges from 0 to 30 volts (by design). The highest value for the friction coefficient and the lowest values for the voltage were chosen to model the behavior of the microsystem in the worst-case scenario (maximum value friction and relatively low values for the dominant electrostatic force). The length of the track in the linear microactuator being studied is 1,000 microns, therefore the focus was on the behavior of the device in a range of this order of magnitude. The following graphs of displacement and velocity show the behavior of the device on a range much bigger than that (order of tens of millimeter) in order to get an idea about the overall behavior of the device assuming a relatively large track for the shuttle to travel on (keeping in mind that some of the applications this electrostatically driven linear microactuator might be used and would normally require shuttle tracks several millimeters long).

Now looking at the velocity and displacement of the shuttle in a range of 0 to 2000 microns, which is the same order of magnitude as that of the track of the device, the following graphs are obtained:

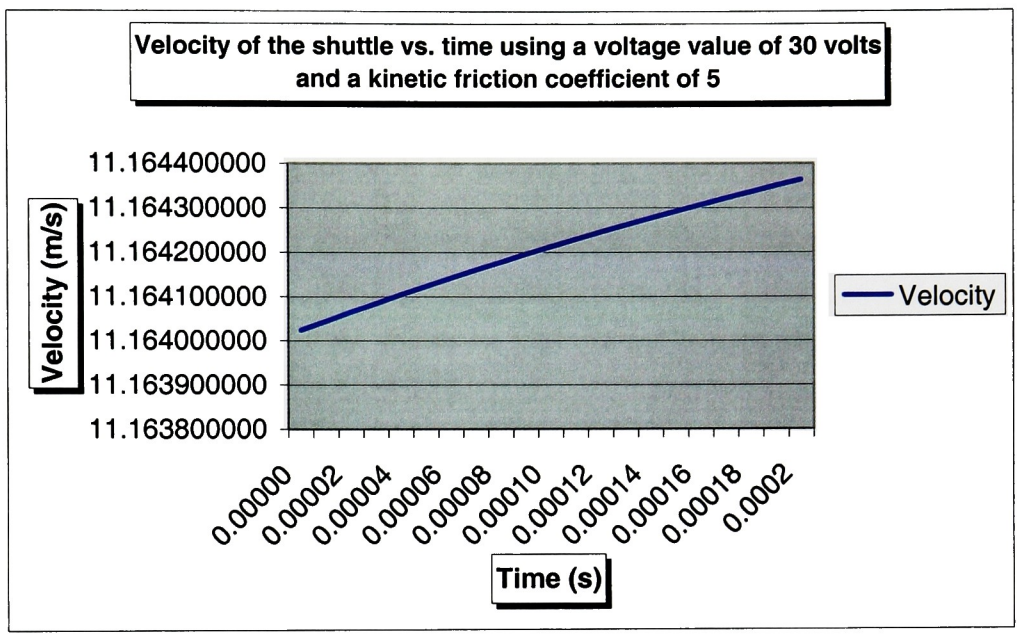


**Figure 16. Velocity of the vehicle vs. time using a voltage value of 30 volts and a kinetic friction coefficient of 5 (1st 2000 microns).**

Figure 16 above shows the velocity profile of the shuttle as a function of time. The shuttle has an increasingly linear motion over the time interval [0.01 ms, 0.18]. Another observation that can be made is that the magnitude of the velocity does not change a lot over this period of time. For instance, at time 0.04 ms., the velocity has a magnitude of about 11.1641 m/s, and at time 0.18 ms the value for the velocity is only 11.1643. Thus, the total velocity increase over this time interval ([0004 ms, 0.18 ms]) is only 0.0002 m/s, which is not very significant, especially, if the velocity is plotted over a time interval of few milliseconds as it is discussed later.

Shown below is Figure 17 for the corresponding profile for the displacement over the same time interval. Theoretically the profile for the displacement of the shuttle over this time interval should not be linear; rather concave upward. However, since the increase in the velocity is so small, it is difficult to see that concaved shape considering the time increments used are 0.1 ms.. A more accurate plot could be drawn using smaller time increments. The displacement profile in Figure is show to be linear, which is not exactly accurate.

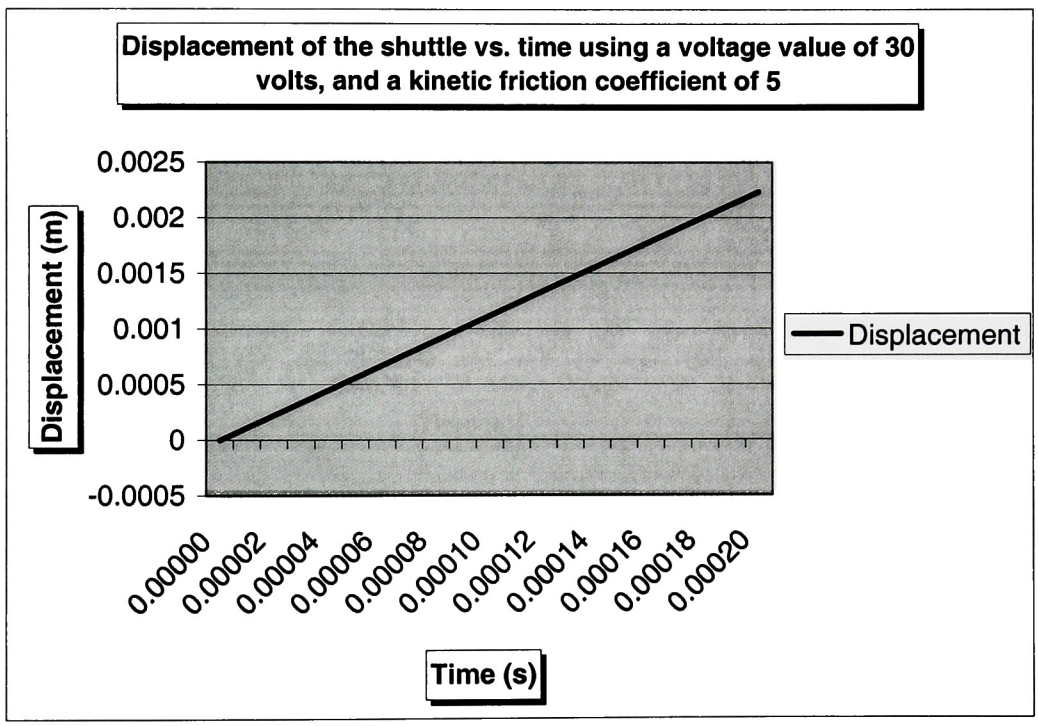


**Figure 17. Displacement of the shuttle vs. time using a voltage value of 30 volts, and a kinetic friction coefficient of 5 (1st 2000 microns).**

Even at low voltage values, the calculations performed, as it is discussed below, show that the shuttle moves a distance of about 1000 microns in less than 0.1 milliseconds. Thus, the time increments used to plot the different graphs were 0.1 and 0.2 ms, and the corresponding time interval used for this analysis is 0 to 5 milliseconds.

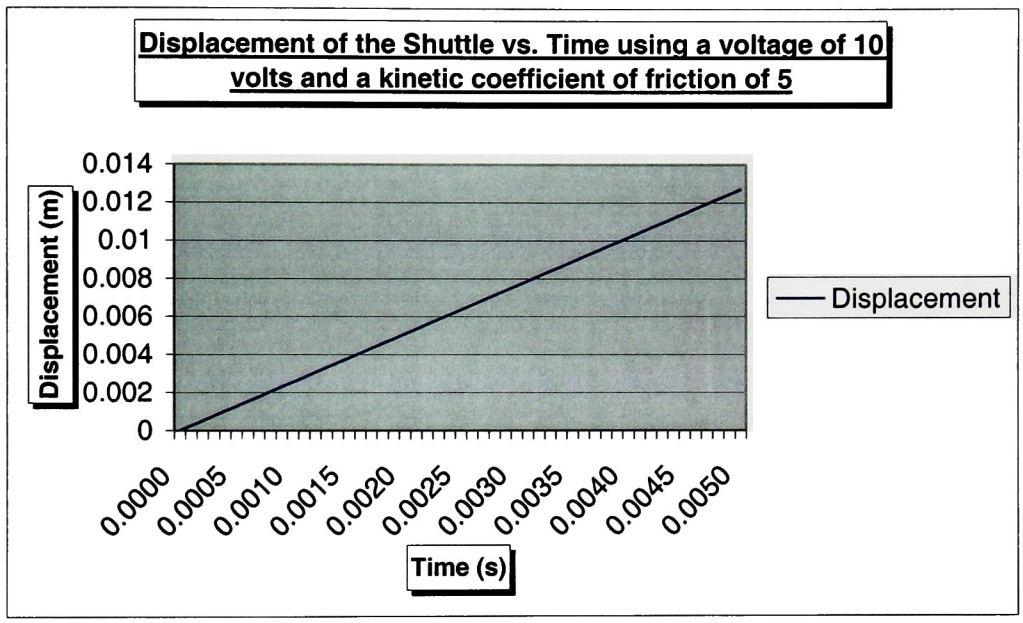


**Figure 18. Displacement of the Shuttle vs. Time using a kinetic friction coefficient of 5 and a voltage value of 10 volts for the time interval of [0, 5 ms]**

Figure 18 shows that applying a voltage value of 10 volts and the highest value for the kinetic coefficient of friction (the value 5 being, as was discussed earlier, the highest value for the coefficient of friction reported in research experiments performed by different researchers for such devices), the displacement linearly increases as a function of time. This figure shows the distance being covered to be from zero to twelve millimeters, which is much bigger than the distance the shuttle is designed to cover (1000 microns). Again, it

is important to remember that the theoretical profile for the displacement is not exactly linear since the velocity over this period of time is not constant, but increases very slightly as it is shown if Figure 19 below.

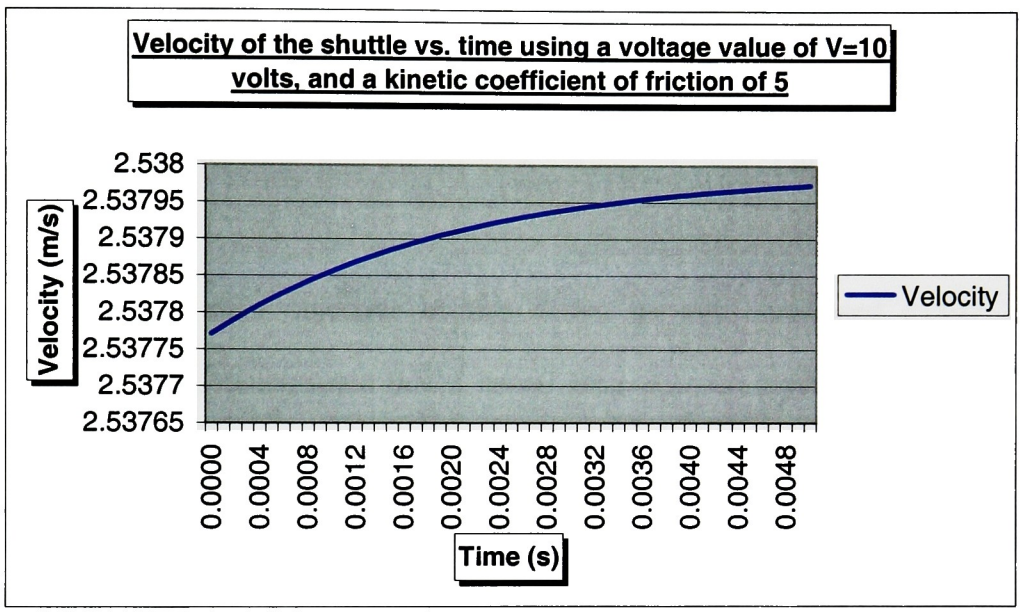


**Figure 19. Velocity of the Shuttle vs. Time using a Kinetic friction coefficient of 5 and a voltage value of 10 volts for the time interval of [0, 5 ms]**

Figure 19 illustrates the behavior of the velocity as a function of time in the same time interval from 0 to 5 ms.. There are two main observations to be made in this case. The first observation is that the velocity does increase over the time interval [0 ms, 5 ms]. This behavior of the velocity, illustrated by the velocity profile above, is exactly what is expected from such a device to show under normal operation conditions. The second observation is that the magnitude of the velocity does not change but very slightly over this time (For instance, at time 0.4 ms, the velocity's magnitude is about 2.5378 m/s, and at time 3.2 ms its magnitude is equal to about 2.5379 m/s—a change of less than 0.0001 m/s). The

reason being is because, when the shuttle is stationary, and after the voltage is applied, the electrostatic force builds up to a value that allows it to overcome static friction (the largest static friction value for such a device is less than $4.9 \pm 1$ as was reported earlier). After such a point, the shuttle starts moving and the frictional resistance decreases, which it, generally, does. Then the kinetic frictional resistance stays about constant, and so does the velocity. The acceleration becomes null and the device reaches a state of dynamic equilibrium.

The main objective of this thesis, as was mentioned earlier, is to, theoretically, demonstrate that a lateral long distance traveling electrostatically driven microactuator can operate upon the application of a certain voltage. The device was designed to have a 1,000 microns long track, on which the shuttle is supposed to travel. The shuttle itself is designed to be 104 microns long, 38 microns wide, and 2 microns thick. No specific application for the device is intended in this thesis. The operation of this device would be the shuttle moving on the fixed track due to the electrostatic force generated upon the application of a bias voltage. That is why for the intended objective, studying the behavior of the shuttle on a 1,000 microns long track is all that is needed. However, it was opted to look at how the shuttle behaves in a much longer range (0-15 mm). The purpose of this generalized analysis is to help the experimenter, or the analyst understand the applicability of such a device in a future application, which might require a much longer track than the one designed in this thesis.

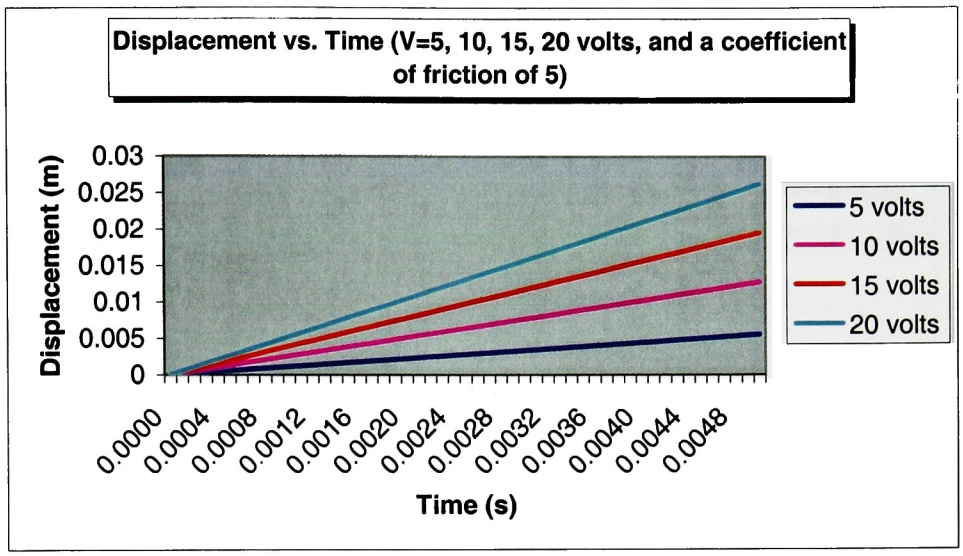


**Figure 20. Displacement of the shuttle versus time, using a coefficient of friction value of 5, and voltage values of 5, 10, 15, and 20 volts.**

It is obvious from Figure 20 that as the value of the voltage applied increases, the slope of the "linear" (It show as linear on the Figure 20, but theoretically it is not, since the velocity over this time interval in not constant, but slightly increases) displacement increases as well. This is the trend that is expected, since the electrostatic force that is responsible for moving the electromechanical device is a function of the voltage squared. So, as the figure above illustrates, at 20 volts the shuttle covers four times the distance it covers when only 5 volts is applied.

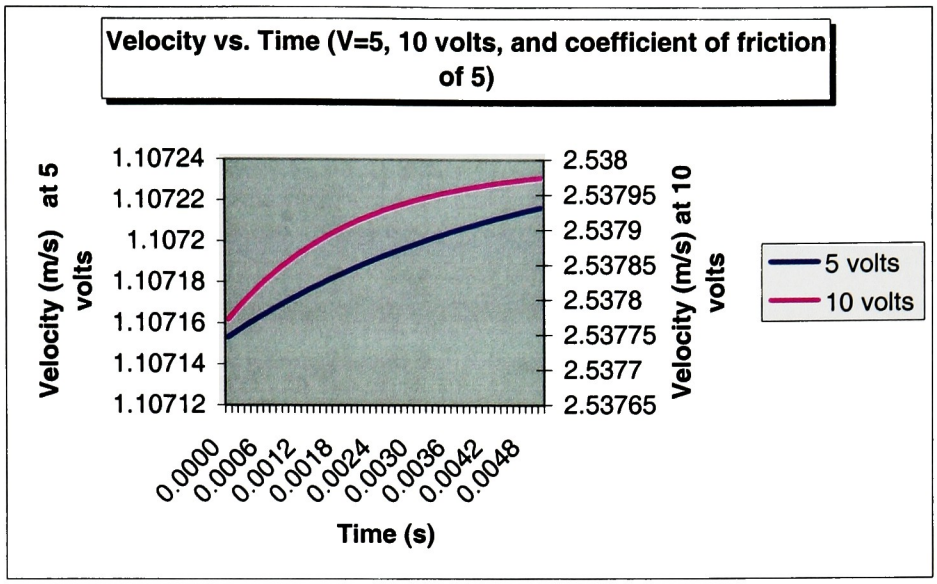


**Figure 21. Velocity of the shuttle versus time, using a coefficient of friction value of 5, and voltage values of 5, and 10 volts.**

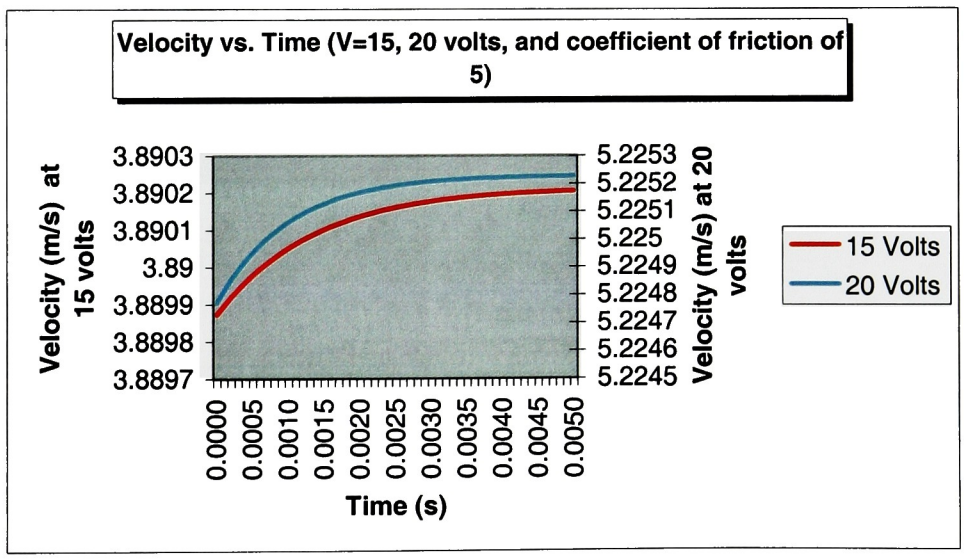


**Figure 22.a. Velocity of the shuttle versus time, using a coefficient of friction value of 5, and voltage values of 15, and 20 volts (Tow different scales)**

Figures 21 and 22.a are plots of velocity versus time at different values of the voltage. Notice that in each figure two different scales are used in order to show

the actual velocity profiles. If the data for the velocity for both voltage values are plotted using the same scale, the profiles will show as two horizontal lines parallel (Figure 22.b) to each other giving the impression that the velocity is constant. The reason for this is because only a very small increase in velocity takes place). It is expected, in the case of an electrostatically driven device, for the velocity of the moving electrode to boost as the voltage is amplified. This conduct is very well pointed up by the velocity profiles shown in Figures 21 and 22.

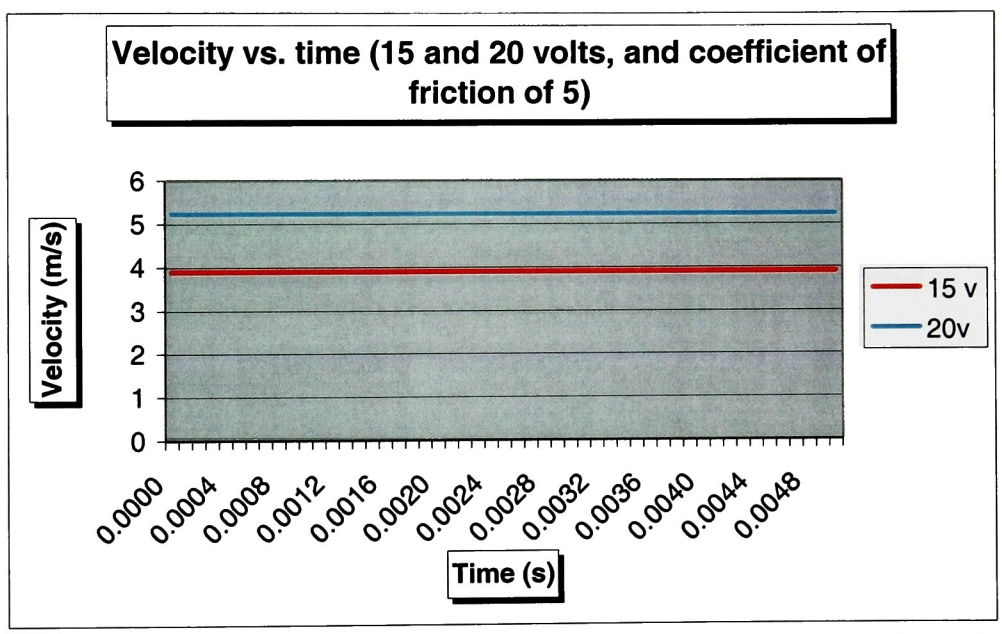


**Figure 22.b. Velocity of the shuttle versus time, using a coefficient of friction value of 5, and voltage values of 15, and 20 volts (one scale)**

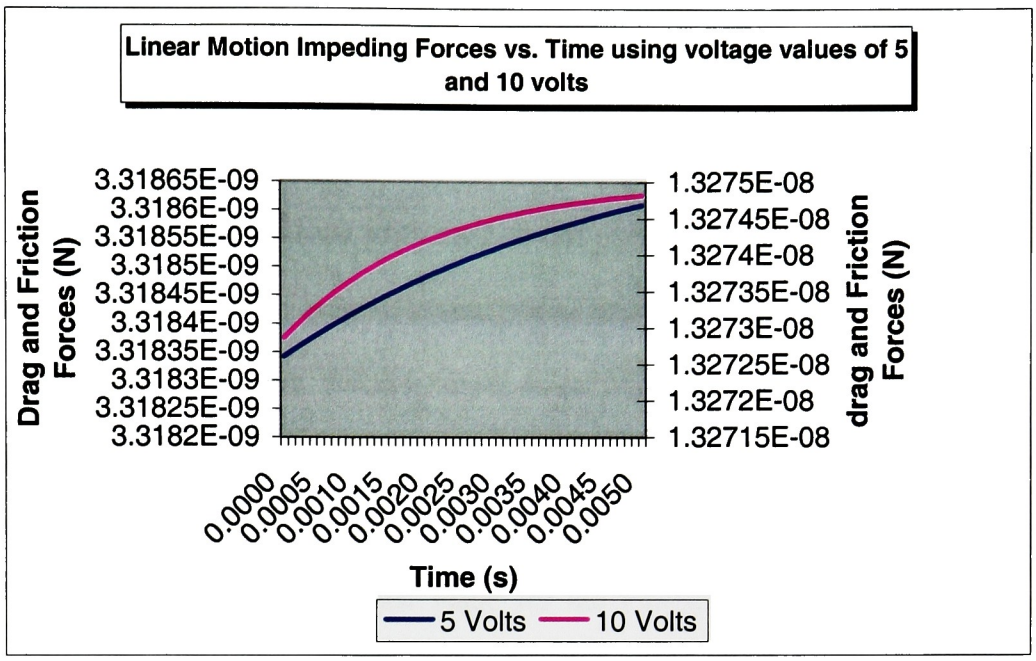


**Figure 23. Drag and friction forces as a function of time for voltage values of 5, and 10 volts.**

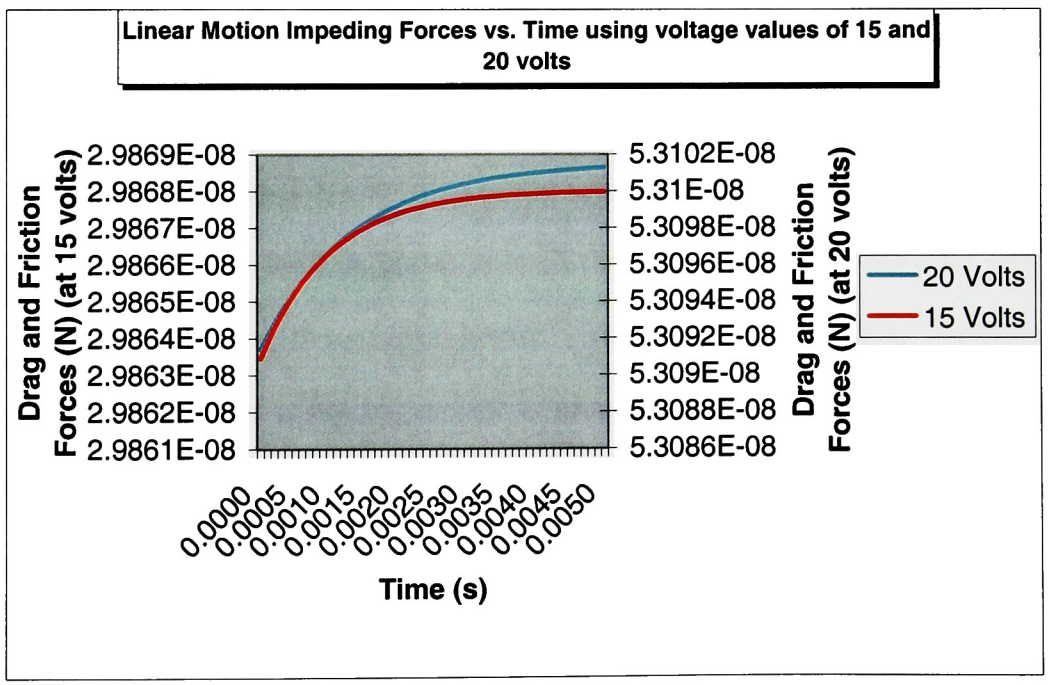


**Figure 24. Drag and friction forces as a function of time for voltage values of 15, and 20 volts.**

In an earlier discussion, it was mentioned that the main forces impeding the motion of the shuttle while it is traveling on the track are the dry friction and the drag forces. Since no such micromachine has been built before, and no experimental work has been performed on this particular type of laterally operated electrostatically driven microactuator, it was important to model these forces to see how the change in voltage would affect their magnitude, and in turn the operation of the device. Figures 23 and 24 are the evidence of the projected performance of these forces over the duration of the shuttle travel on the flat track. In this case, the largest value for the kinetic coefficient of friction is assumed, and different values for the voltage were used to see the effect of voltage on the magnitude of these forces, which serve to hinder the motion of the device, and eventually bring it to a standstill. With a fixed value for the coefficient of friction, the dry friction force is constant. The drag force, however, is not constant, since it is a function of the velocity squared. So, as the velocity increases, the drag force increases as well, and this trend can easily be seen demonstrated in the two graphs above. The magnitude of these 'motion-encumbering' forces is not big enough to bring the shuttle to a halt in the time interval during which the shuttle travels. Even at very low voltage values (e.g. 5 volts) the electrostatic force accountable for moving the shuttle remains dominant, and capable of overcoming the static friction, the dry friction, and drag forces. So, for the purpose of getting the shuttle to move on a horizontal flat track without staling, a voltage magnitude of 5 volts is enough, assuming the shuttle is carrying no load. Of course, for any applications of such a device where carrying a load is

important, larger voltage values would need to be applied in order to get the shuttle moving. These voltage values could be easily determined if the weight, size, and structure of the load is known.

## 3.2. Excitation Scheme:

Actuation of the linear micromotor is performed by electrostatic force, which is exerted between three stator electrodes and three movable poles at any given time. At any given time there are three terminals (sets of tow opposing electrodes-one stator and one movable pole), which are partially overlapped, and three terminals, which are completely overlapped. More specifically, six of the shuttle poles (3 from each side) already have an overlap with twelve stator electrodes (6 from each side) of the next active phase.

In order to get a continuous shift of the moving electrode (shuttle), it is important to use a three-phase power generator with controlled frequencies. The conventional excitation sequence generated by this power generator consists of successive activation of three partially overlapped terminals (one phase). The electrodes structures are operated with this 3-phase circuit, which is capable of output voltages from 5 to 30 volts with maximum frequencies $f_0$ ranging from zero to 183.3 KHz and 1860 KHz respectively. The values obtained for these frequencies are based on the periods (time to perform one cycle) calculated corresponding to the distance covered by the partially overlapping poles from one phase to the other. This distance covered is always 6 microns by design. The speed with which the phases change from one to the other depends on the

magnitude of the voltage applied. So, for instance, at a voltage of 5 volts, the corresponding velocity would be 1.10 m/s and the excitation frequency required in this case would need to be 183.3 KHz. These values for the frequencies are somewhat high, which is due to the relatively elevated voltages applied. If such a power generator with frequency control is not used to create this multi-phase sequence, the shuttle will only travel a distance of 6 microns, which is the maximum overlapping distance between poles, and then stop. Therefore, to keep the shuttle moving continuously, the frequency needs to be increased as the voltage augments, since a voltage increase results in a simultaneous velocity boost.

A sample excitation scheme by which electrodes of different phases are activated at different times in a periodic manner with a frequency $f_0$ is shown below. MATLAB software package was used to generate the square waves illustrating the three-excitation phases. The cases shown below all depict a constant voltage and a period $1/f_0$.

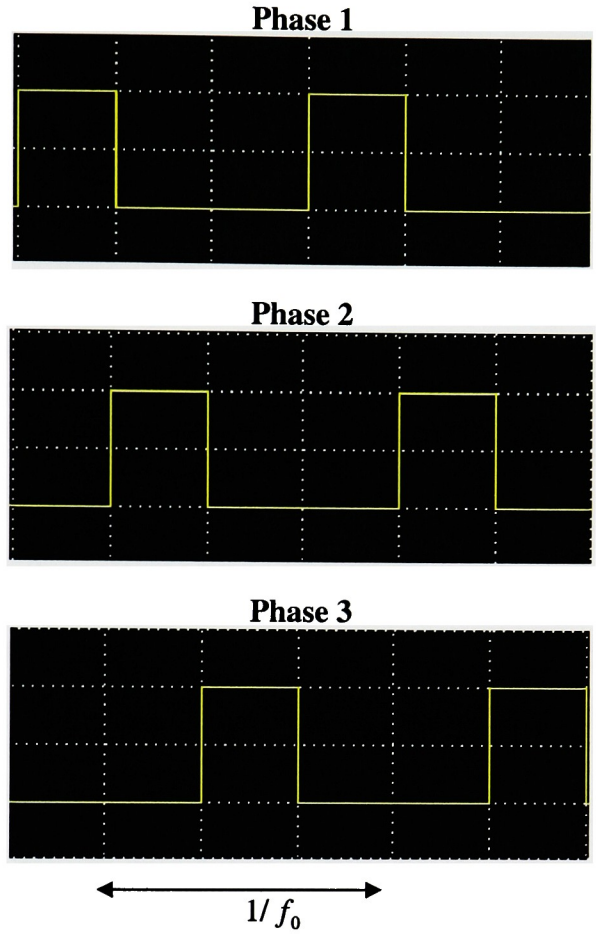


**Figure 25. Excitation Scheme for Linear Motion of the Microactuator**

## 3.3. Breakdown voltage [25]

The mechanism of an electrical breakdown (the maximum voltage at which a capacitor can be used) in an electrostatic microactuator was studied [25] in order to apply large voltage. Weak light emission caused by the ionization process of gas can be imaged using high sensitive (photon counting) CCD camera. Silicon-to-silicon gap configuration showed a higher breakdown threshold than metal-to-silicon gap. Departure of breakdown from the Paschen's curve (see Figure 25) appears in the metal-to-silicon configuration, but not in the

silicon-to-silicon as shown in Figure 25. It suggests that secondary electron emission from the metal has an influence on the low breakdown voltage.

The following graph shows the breakdown voltage measured for polysilicon on polysilicon in electrostatic microactuators. In the design of the electrostatic microactuator being studied in this thesis, the gap between the poly layers is kept at 2 microns, for optimum functionality of the micromachine, design reasons, and in consideration of the manufacturing capabilities here at RIT. At this silicon-to-silicon gap of 2 microns, the breakdown voltage is about 350 volts, which is a much higher voltage value than the magnitudes used in this current design (5V – 30 Volts). The voltage values used in the design of the linear microactuator are in the order of 10 volts, and are far below the breakdown values measured for poly-on-poly layers with a gap of 2 microns. The breakdwon voltage is, therefore, a non-issue in the current design. Even the metal-to-silicon gap breakdown voltage at such a small gap of 2 microns is still much larger than the voltage designed to be used to operate the linear microactuator device.

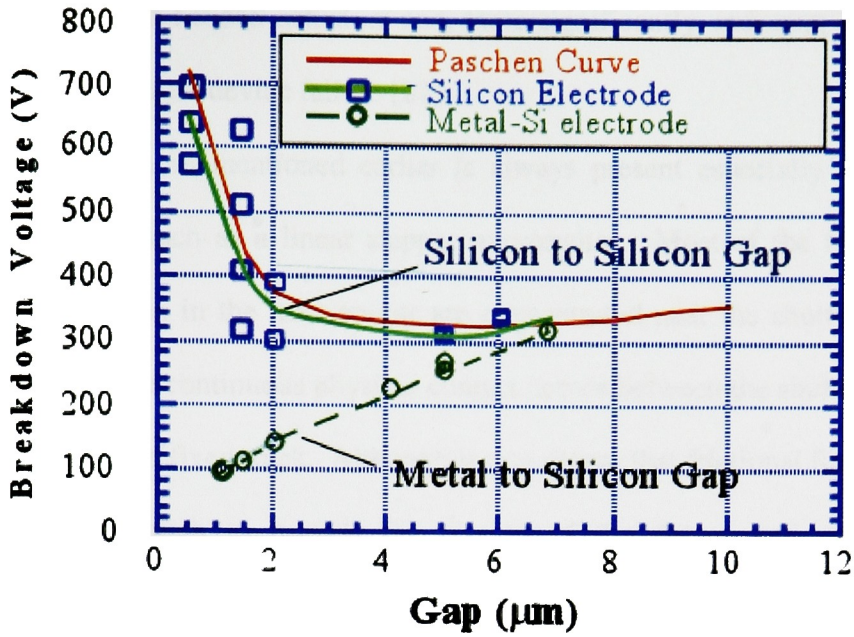


**Figure 26. Breakdown voltage measured using elctrostatic microactuator [25]**

## 3.3. Lubrication

A peculiar feature of MEMS devices is that the surface roughness of the material used can become a significant factor in the overall device geometry. MEMS surface finishes are quite varied, ranging from atomically smooth surfaces found on polished single-crystal silicon substrates to the rough surfaces left by different etching processes. The effects of these topologies can be important in several areas for microdevice performance [26].

Friction is a relatively uncharacterized property of Micro-Electro-Mechanical Systems (MEMS) that can significantly impact both their performance and reliability. Frictional effects include both increasing the power

requirements of MEMS actuators and, more significantly, inducing wear that can result in premature device failure [27].

Friction as mentioned earlier is always present especially in side drive micromotors, such as a linear stepper micromotor. Most of the friction forces resisting motion in the micromotor are concentrated near the shuttle-fixed track interface where continuous physical contact occurs between the shuttle supporting dimples and the fixed track. Although it was shown that frictional forces were not significant enough to impede the motion of the device and prevent linear translation of the shuttle, it would still be wise to apply some sort of lubricant to minimize this friction without hindering the microactuator's performance.

Research [22] has shown that for unlubricated surfaces, more menisci are formed at higher humidity resulting in higher friction force between the surfaces. The formation of meniscus (Capillary condensation of water vapor from the environment results in formation of meniscus bridges between contacting and near contacting asperities or rough surfaces) forces is supported by the fact that the static friction force for unlubricated micromotors increases at high humidity. Therefore using a lubricant such as a bonded layer of Z-DOL (wet lubricant often used to minimize friction is hard drives) can provide good lubrication to the micromotor by reducing the static friction [22]. A layer of 1 or 2 nanometers thick of such a lubricant would suffice to minimize frictional forces in a micromotor. The micromotor could be submerged in a liquid lubricant, which would result in what is called a fully flooded lubrication regime [28], but such method is not practical in this case since the shuttle is supposed to be operating in

air under atmospheric pressure. If the fully flooded lubrication regime is applied, then only the viscous contribution to the friction forces would be relevant. The meniscus forces become immaterial in this case.

# Chapter IV – Process Flow

## 4.1. Fabrication Laboratory

The Semiconductor & Microsystems Fabrication Laboratory, and facilities at RIT have all the tools necessary for the manufacturing of different types of MEMS devices. Devices including, but not limited to, deep trench structures and surface-machined micro-mirrors, cantilevers, sensors and transducers, and microfluidic transport structures. Electrical devices, such as Bipolar and MOS (PMOS and CMOS) processes are also done at these facilities.

The design of a process flow for the manufacturing of this linear electrostatically driven microactuator is part of this thesis although its manufacturing is not. Therefore, since, this device is to eventually be fabricated at the RIT facilities, the following flow process was developed with that in mind.

## 4.2. Design Layout

The design layout of the MEMS device in question was done using the Mentor Graphics CAD tool available in the RIT VLSI laboratory facilities. Since this MEMS device has never been manufactured before, several different designs were attempted with different parameters and dimensions. They were analytically tested to see if they are operationally feasible, and a final design has been chosen. Below is a picture of the design layout of the long distance traveling laterally operated electrostatically driven micro-actuator. It is a top view of the layout.

There are several layers to this design all of which are color coded to facilitate mask designs.

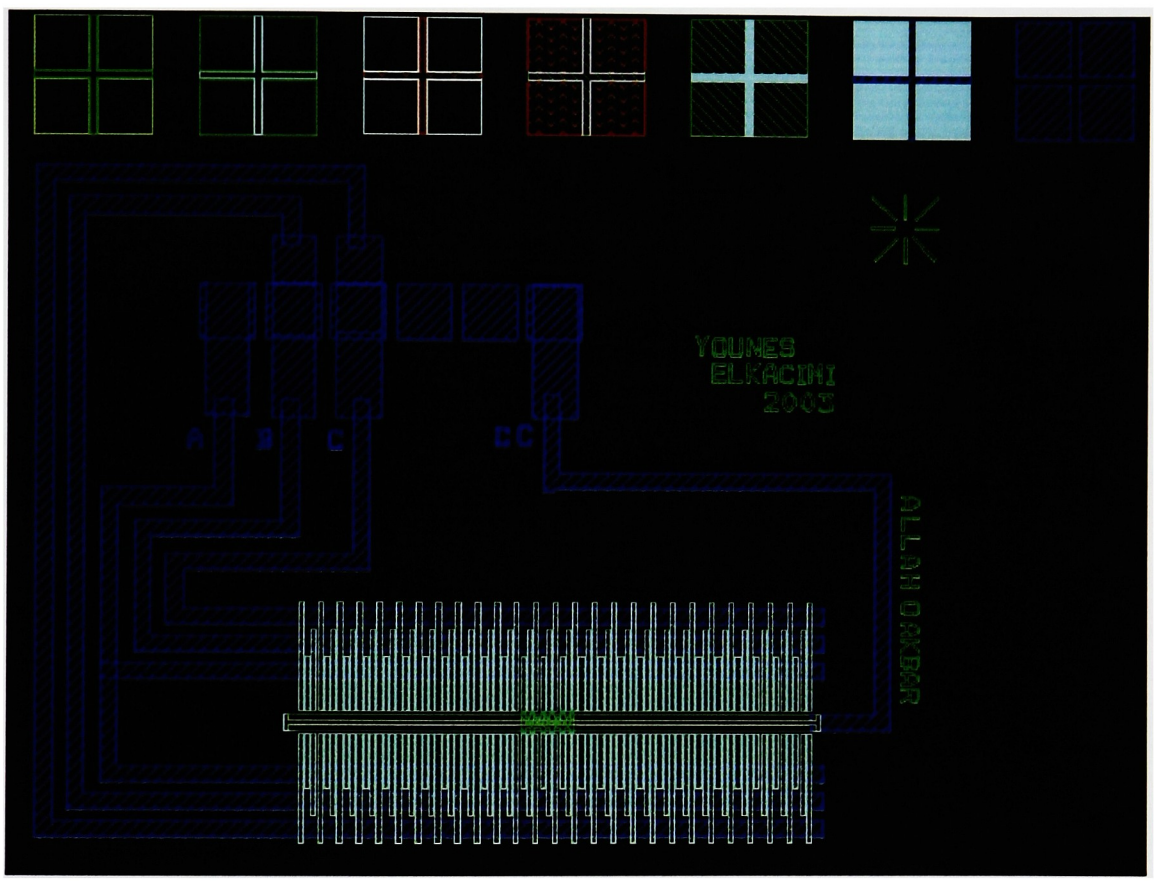


**Figure 27. Mentor Graphic Design of the Electrostatically- Driven Microactuator (Showing all layers)**

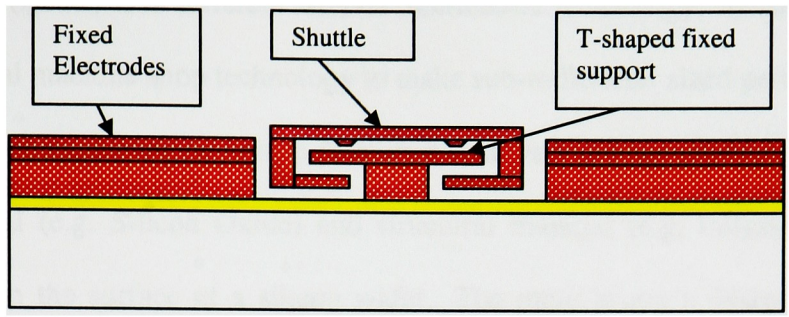


**Figure 28. Cross sectional area of the MEMS device (track and shuttle)**

## 4.3. Silicon Surface Micromachining

There are a number of MEMS micro fabrication technologies that have been developed over the years. These technologies make devices ranging in size from a dozen millimeters to a dozen microns. Microfabrication was initially based on planar silicon techniques, such as bulk and surface micromachining that were derived from microelectronic technology. Silicon surface micromachining inexpensively makes completely assembled mechanical systems. Silicon bulk micromachining uses either etches that stop on the crystallographic planes of a silicon wafer or etches that act isotropically to generate mechanical parts. These techniques combined with wafer bonding and boron diffusion allows complex mechanical devices to be fabricated. Another very useful fabrication technology, the LIGA (in German, Lithographie, Galvanoformung, Abformung) technology uses lithography, electroplating, and molding processes to produce microstructures and miniature parts with great accuracy. Electro Discharge

Machining (EDM) is a different MEMS fabrication technology, which extends conventional machine shop technology to make sub-millimeter sized parts.

Surface micromachining technique follows a relatively simple principle. Layers of sacrificial (e.g. Silicon Oxide) and structural material (e.g. Polysilicon) are deposited on the surface of a silicon wafer. The more layers a design has, the more complex the structure, and the more difficult it becomes to fabricate. The layers are, then, patterned according to the designer's specifications, and the sacrificial material is removed to leave the now completely formed micromechanical devices. These micromechanical parts or devices generally use a little power to operate, and are very quick to respond. They occupy a small volume, and are often much less expensive than conventional macro parts.

## 4.4. Manufacturing Process

The following are the steps, which should be followed in the manufacturing process of the long distance traveling micro-actuator MEMS device. The flow process is, first, discussed in each step, then the consecutive device cross sectional areas are described in detail to illustrate the different manufacturing steps followed to build the device. Some Mentor Graphic (Software package used to design the different layers of the masks) images are included as well to illustrate the different layouts corresponding to the particular cross sections.

The lectures and presentations of Dr. Lynn Fuller, Motorola Professor at Rochester Institute of Technology were heavily relied on in designing the following fabrication process flow for this linear electrostatically driven microactuator.

### 1. Start/ Scribe

In this first step, a lot number is scribed and RCA (Radio Corporation of America) clean is performed as described in the following steps:

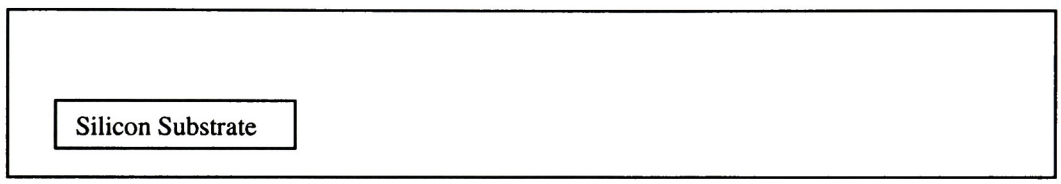


**Figure 29. Bare Silicon Substrate**

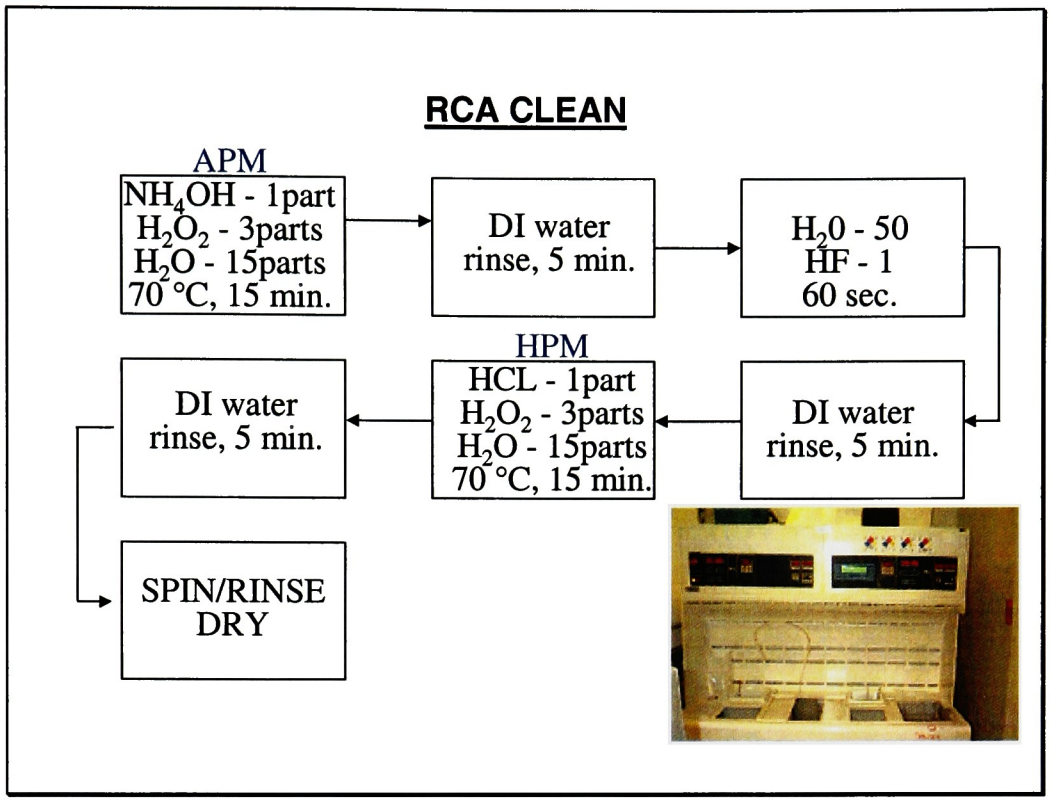


**Figure 30. RCA Clean Procedure and Tool [29]**

**2. Deposit a layer of Silicon Nitride**

This nitride layer will serve as an etch stopper, because towards the end of the fabrication process, releasing the shuttle will require etching the sacrificial oxide. If Low Temperature Oxide is used for this layer instead of Nitride (Si3N4), then this layer would be etched and thus, possibly, exposing the silicon substrate to the etching agent. The latter is not a sought-after effect.

The following recipe needs to be followed in order to deposit the required thickness (3500 Å) of silicon nitride:

- 6" LPCVD Tool – Recipe Nitride810
- Thickness: ~ 3500 Å Silicon Nitride Si3N4
- Temp = 810°C

•DiChlorosilane Flow 60%

•Ammonia 60% flow

•Time =70 min.

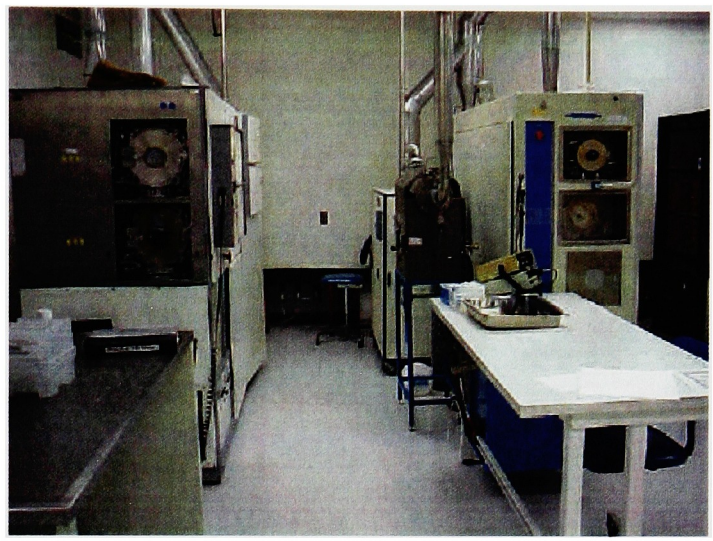

**Figure 31. (LPCVD) Low Pressure Chemical Vapor Deposition Tool**

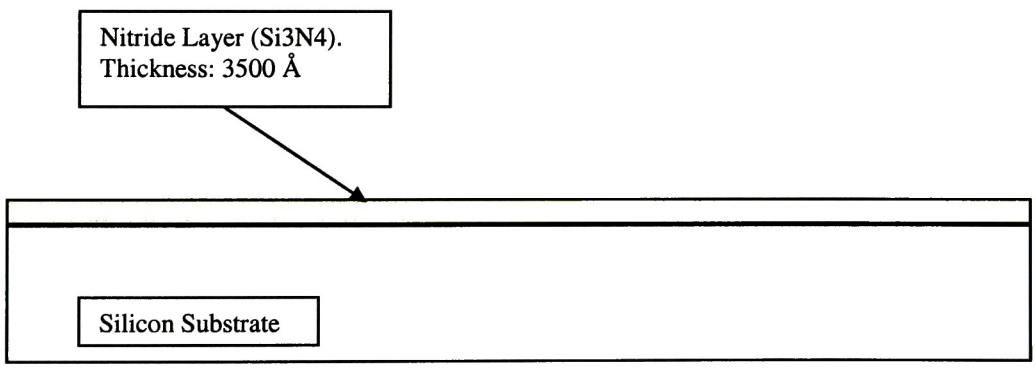


**Figure 32. Nitride Deposition**

### 3. Deposit the first layer of poly-silicon.

This layer of Poly Silicon is the first of three poly-silicon layers to be deposited. This layer, after being patterned, serves as the base for the fixed support. This support is a fixed conductive electrode anchored to the silicon substrate on the Nitride layer. Besides carrying the shuttle, this fixed support

supplies voltage to the shuttle. The first layer of poly is deposited and is 6 microns thick. The poly is then doped to make it conductive.

The following tool and recipe are used for polysilicon deposition:

- 6" LPCVD Tool
- Thickness: ~ 60,000 Å Poly Silicon
- Temp = 650 °C
- Pressure = 330 mTorr
- Silane Flow 48%
- Dep Rate = 235 Å/min
- Time = 4hr 26 min

It may be difficult to measure the poly thickness, because of the underlying layer of nitride. A monitor wafer with 1000 Å of oxide should be included in order to use the 'Nanospec' measurement tool.

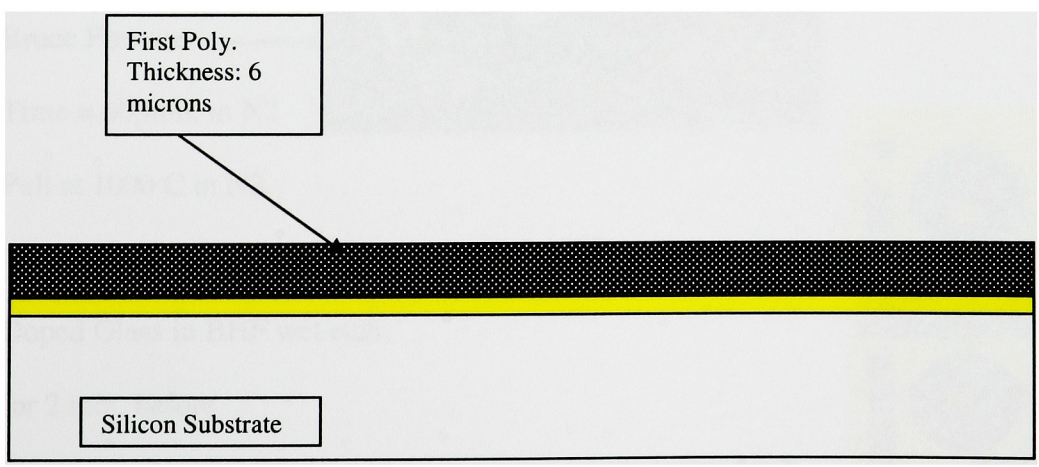


**Figure 33. First Poly layer Deposition**

### 4. N+ Doping of First poly

The objective is to dope the first layer of polysilicon n+ so it will be conductive. A spin-on glass dopant source is used along with high temperature diffusion process to allow dopant atoms to diffuse from the spin-on glass into the polysilicon. The spin-on glass will be etched off and the sheet resistance will be measured using a four-point probe technique.

The following steps need to be followed in order to accomplish this part of the fabrication process. First spin coat with Emulsitone, N-250, at 3000 rpm for 30 sec. Then, bake at 200 C for 15 min. After that, use Bruce Furnace Recipe 120. Use Tube 03 or Tube 12 and the following manual sequence:

Push at 900 C in N2

Ramp to 1000 C in N2

Start soak at 990 C

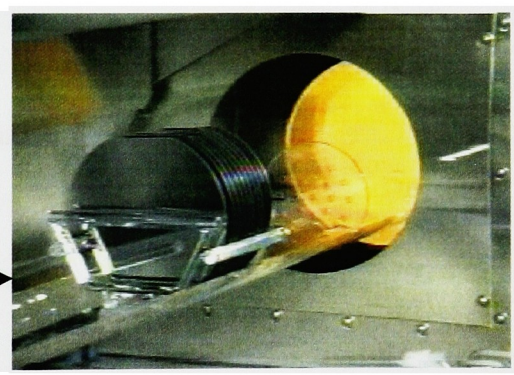

Bruce Furnace →

Time = 60 min. in N2

Pull at 1000 C in N2,

and then etch Phosphorous

Doped Glass in BHF wet etch,

for 2 min, before

the 'Rinse and spin Dry' step. →

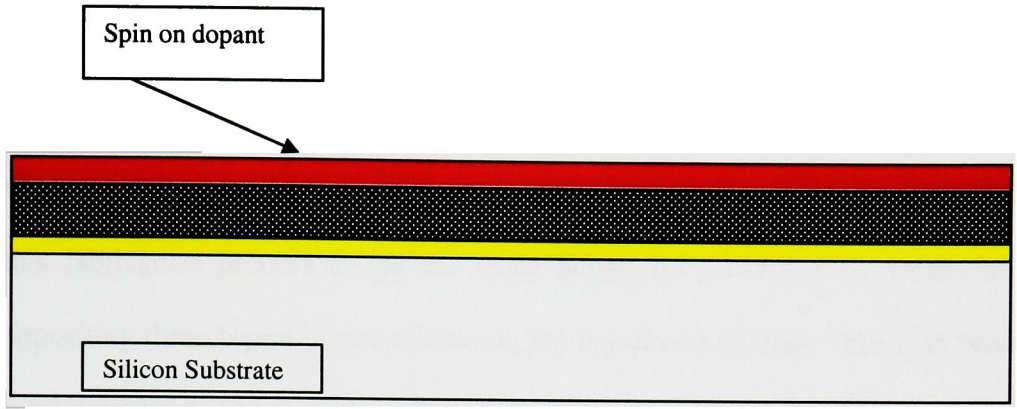


**Figure 34. Doping First Poly**

5. **Remove Spin On Dopant Glass**

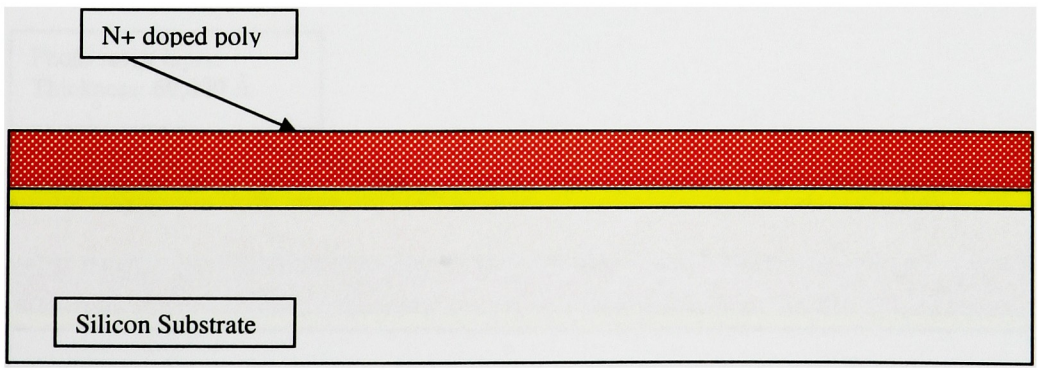


**Figure 35. N+ doped Poly Layer**

### 6. Deposit Photo Resist to etch poly

This is the first lithography step, where the first poly is patterned to create the fixed support for the shuttle along with the fixed electrodes.

The fixed electrodes on both sides of the shuttle are designed to have the same thickness as that of the shuttle (12 microns). Therefore, the technique pursued in this fabrication process to get the exact height for the fixed electrodes is by depositing three layers of polysilicon on the top of one another. The first layer is 6 microns thick and it is deposited at the same time as the fixed support for the shuttle. The other layers will be added as the subsequent poly depositions are made.

To deposit Photo Resist the subsequent steps are to be pursued:

No Dehydration Bake

Coat with ASPR-528 thick photoresist, and dispense 4ml, spread, at 3000 rpm for 1min. Bake at 115 C for 1 min, and then expose in stepper for 1.0 sec. Integrate mode, focus 250. After that develop in CD-26 for approximately 1 min, before the 'Rinse in DI water' and 'Spin Dry' steps

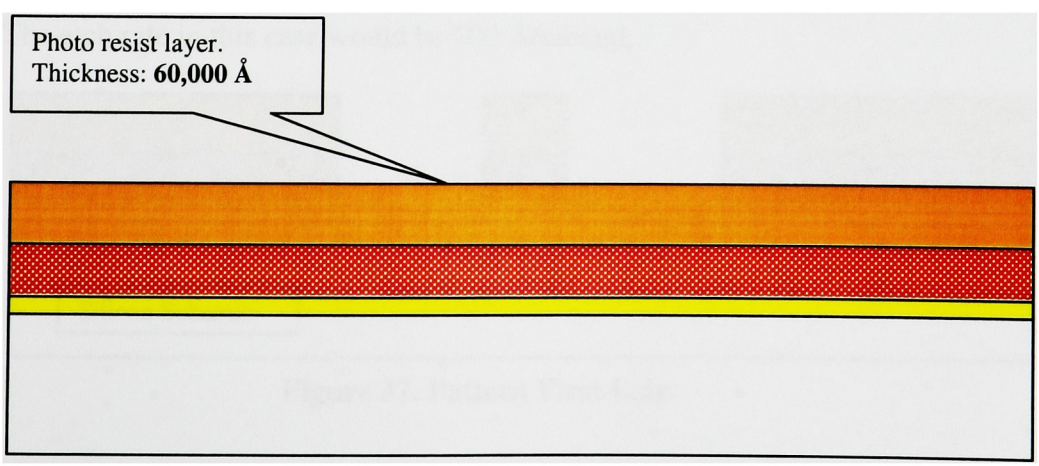


**Figure 36. Photo Resist Deposition**

### 7. Pattern first poly layer

During this lithography step, poly was patterned using a mask designed to leave the parts of the, would be, device that constitute the base of the fixed support and the fixed electrodes on both sides of this support base.

The objective is to etch the 1st layer of polysilicon. The poly is on top of a nitride layer. The etching should be stopped after the poly is etched and before much of the nitride is etched. Otherwise, over etching will cause the nitride to be etched away. Etching of the first poly is performed using Plasma (dry) etching.

Dry Etching:

Dry etching is carried out by using a reactive plasma. The wafer is placed in a reaction chamber, which is then filled with gas containing chlorine, fluorine or other chemistry. The gas is converted into plasma by the power supply. The plasma reacts at the surface of the wafer, and the volatile byproducts are removed by the vacuum pump. The recipe suggested in this fabrication process is the following:

SF6 42.5 sccm, O2 at 7.5 sccm, 400 mTorr, and 40 watts.

The etch rate in this case would be 100 Å/second.

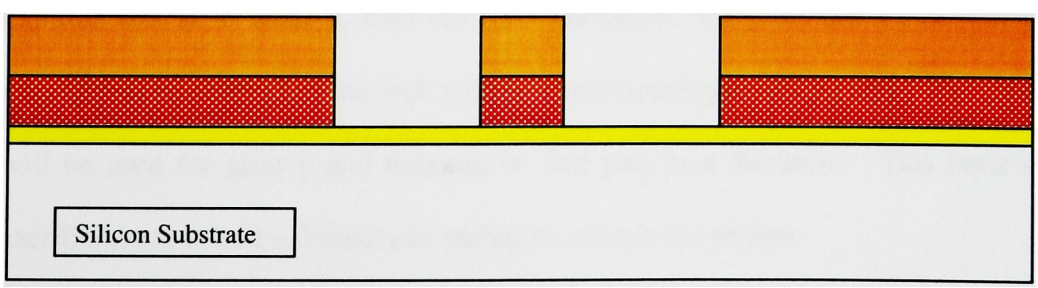


**Figure 37. Pattern First Poly**

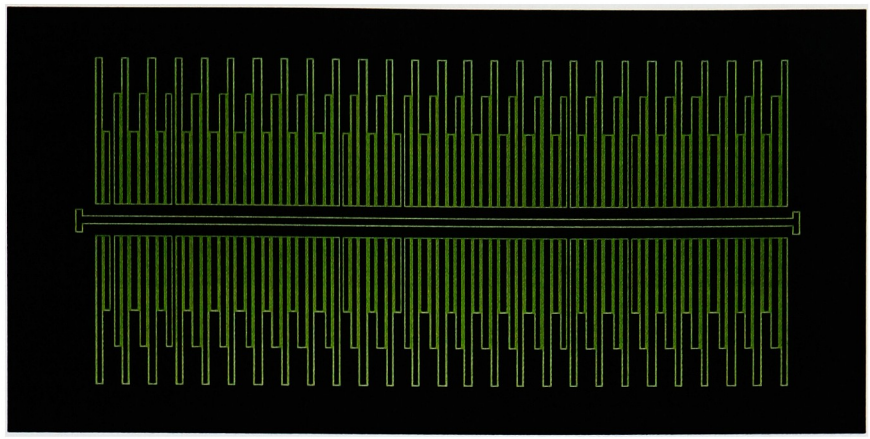

**Figure 38. Top view of the first poly (patterned) shown in this Mentor Graphic Layout (Alignment Marks are not shown).**

### 8. LTO (Low Temperature Oxide) deposition.

The next step is to strip the photo resist in Acetone, rinse in DI water, and blow dry, and then sacrificial oxide can be deposited.

The objective is to deposit a 6.0 microns-thick layer of oxide on the wafer. This oxide is the sacrificial oxide spacer on the top of poly one and under poly two, which will be deposited next.

Since this LTO is on top of nitride and or poly it will be hard to measure the resulting thickness. A couple of bare silicon wafers should be included as monitor wafers in order to find the LTO thickness. One monitor wafer will be step etched to determine the etch rate in a subsequent processing step. The other will be used for groove and measure to find poly two thickness. This layer of sacrificial oxide will ultimately be etched to release the shuttle.

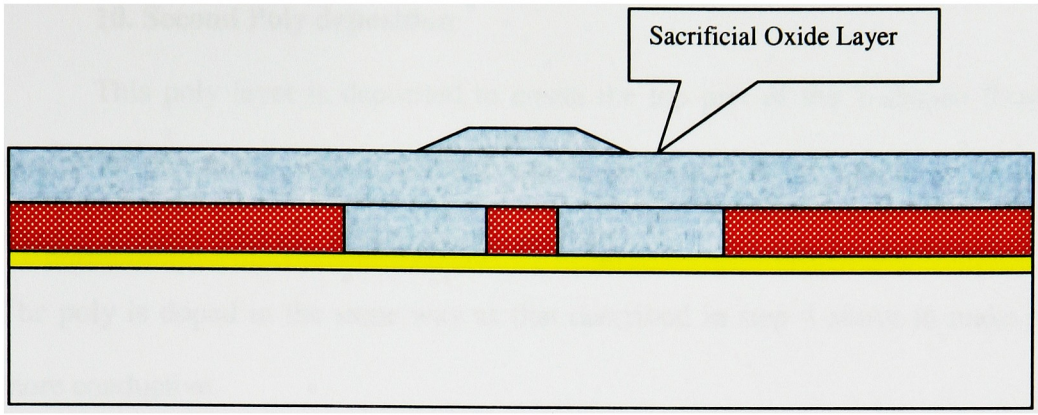


**Figure 39. LTO**

## 9. CMP (Chemical Mechanical Planarization)

This step is needed to planarize the first poly in order to be able to deposit the second poly layer.

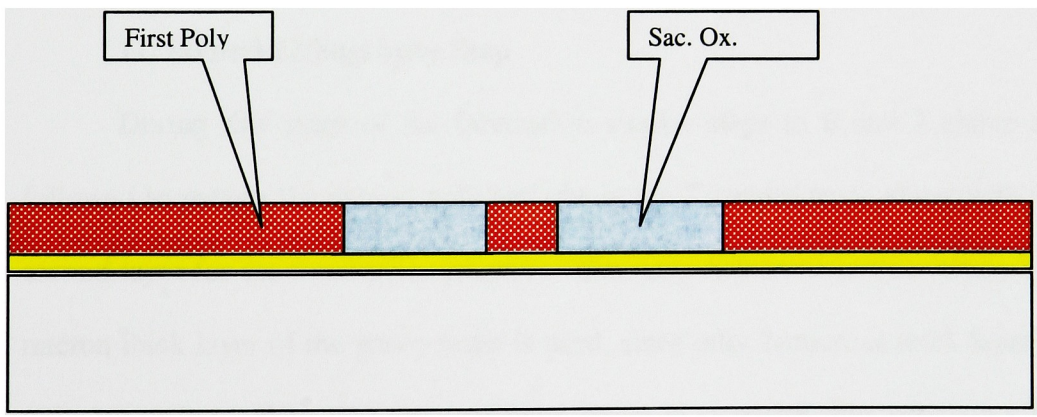


**Figure 40. CMP**

**10. Second Poly deposition**

This poly layer is deposited to create the top part of the T-shaped fixed support of the shuttle, and it also adds one layer of poly to the first layer of the fixed electrodes (Poles). This layer is 2 um thick.

The poly is doped in the same way as that described in step 4 above to make it more conductive.

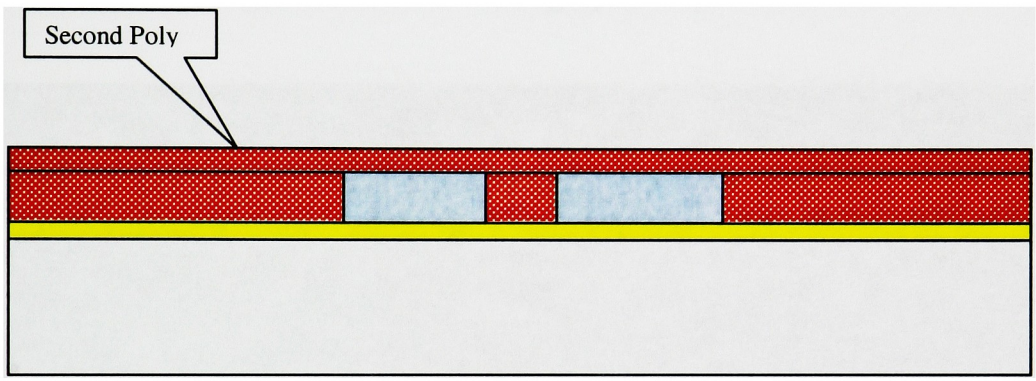


**Figure 41. Second Poly Deposition**

**11. Second Lithography Step**

During this stage of the fabrication similar steps to 6 and 7 above are followed to pattern the second poly and obtain the T-shaped track along with the second layer for the fixed poles (stators). The only difference in this step is a 2-micron thick layer of the photo resist is used, since only 2 microns thick layer of poly is needed. Now that the sacrificial oxide is exposed after patterning the second ploy and performing strip resist, it is etched (step 12) to clear the way for a second LTO deposition.

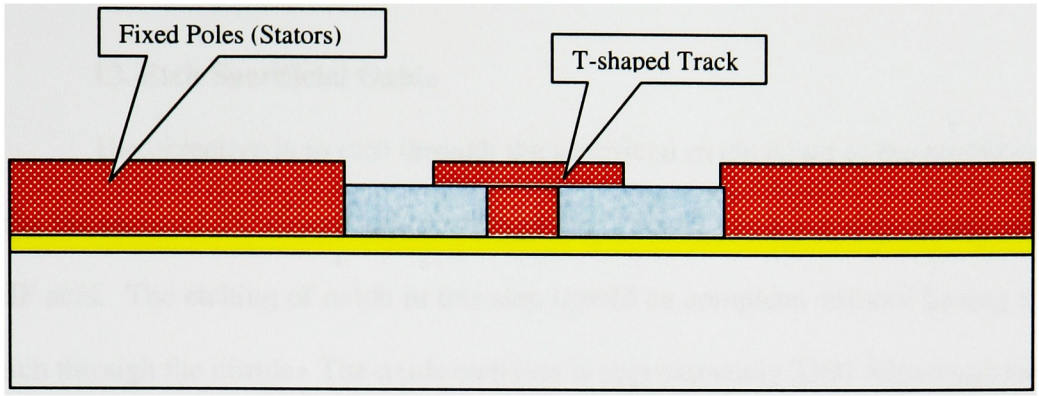


**Figure 42. Second Lithography Step**

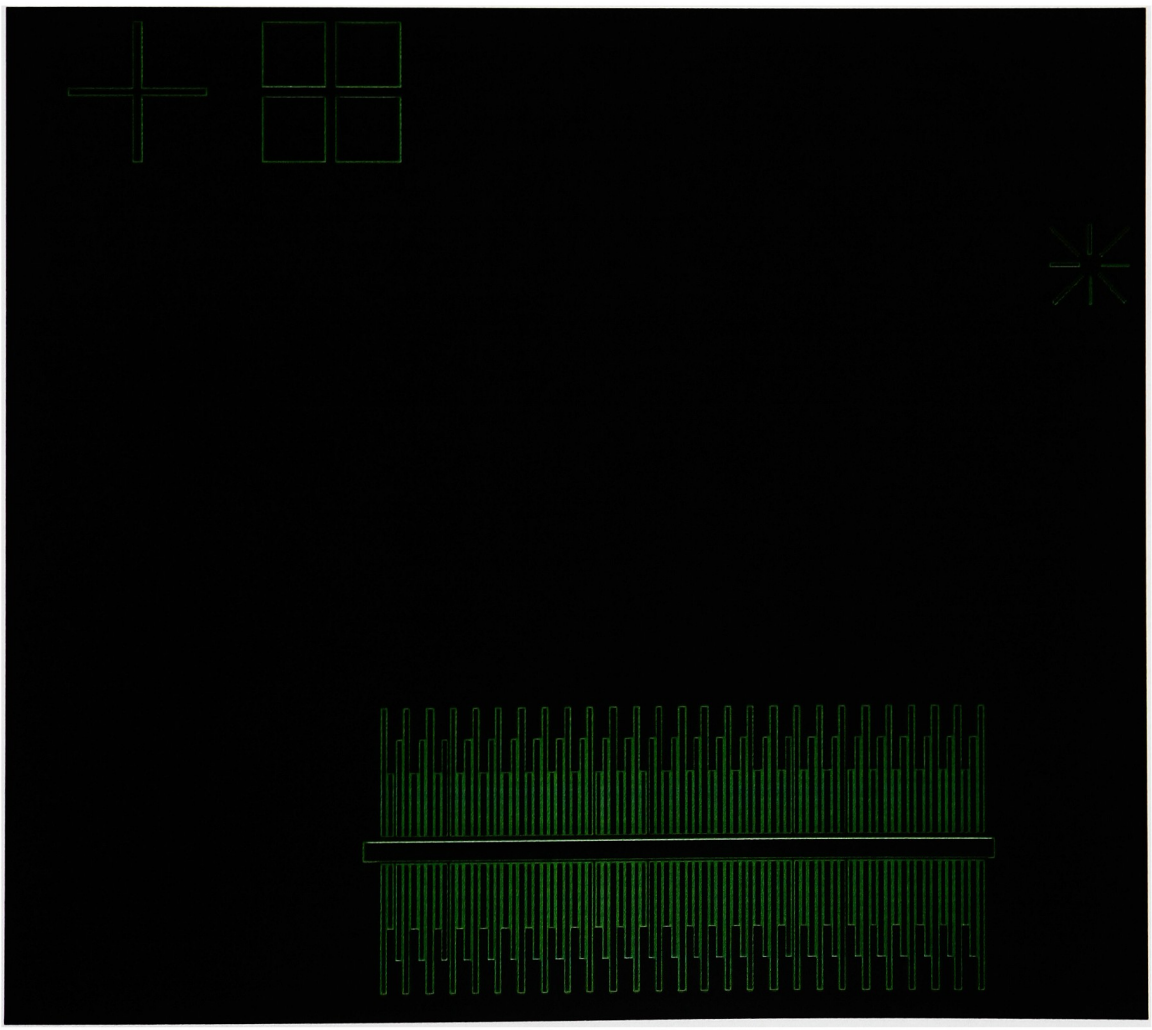

**Figure 43. Top view of the second poly layer (patterned) shown in this Mentor Graphic Layout (Alignment Marks are shown).**

### 12. Etch Sacrificial Oxide

The objective is to etch through the sacrificial oxide down to the nitride so that the second LTO deposition can take place. This etch is a wet etch in buffered HF acid. The etching of oxide in this step should be complete, without having to etch through the nitride. The oxide etch rate is approximately 3300 Å/min and the oxide layer to be etched is about 60,000 Å. The nitride is about 3500 Å thick and the etch rate is about 12 Å/min. The oxide thickness and etch rate are variable so a control wafer (LTO on silicon) should be used to determine the correct etch time. A step etch technique can give accurate results.

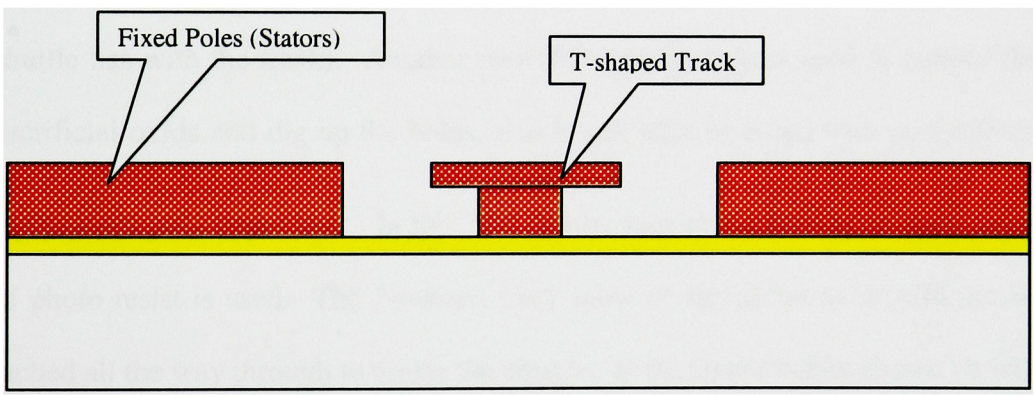


**Figure 44. Etching Sacrificial Oxide**

### 13. Second LTO deposition

This step is needed for conformal coding of the poly with sacrificial oxide. This layer is important to have in order to create the shuttle in the third poly deposition. The shuttle must not be anchored to any part of the track or the fixed poles. It must be free to move on the track with only dimples touching the track.

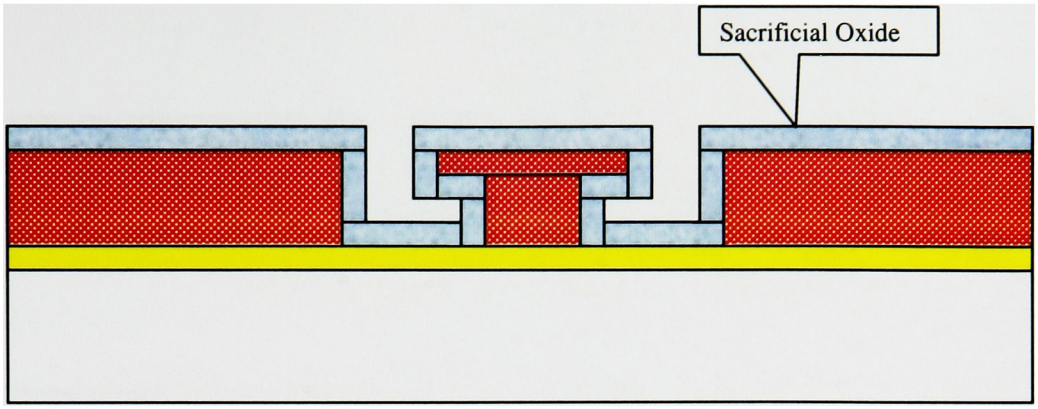


**Figure 45. Second Low Temperature Oxide Deposition**

### 14. Create Dimples

This step is needed to create dimples before the third and the last poly deposition. Dimples will work to help decrease friction between the shuttle and the fixed support, and also to support the shuttle (they are the only contact the shuttle has with the track). Another photolithography step is used to pattern the sacrificial oxide and dig up the holes, which will later be filled with poly-silicon in the third poly deposition. In this lithography step about 40,000 $\mathring{A}$ thick layer of photo resist is used. The 2-micron thick layer of sacrificial oxide will not be etched all the way through to create the dimples as the figure below shows. It will only be etched half way, so that spacing remains between the fixed track and the shuttle (Shuttle will be created in third poly deposition).

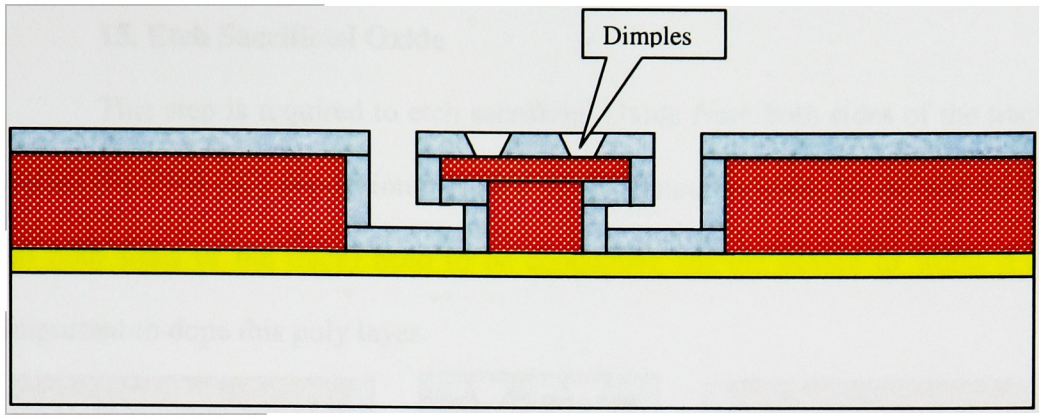


**Figure 46. Dimples**

Dimples are shown in the Mentor Graphics image below as the 2 by 2 micron squares in gray color. This color-coded layer indicates a separate lithography step for creating the dimples.

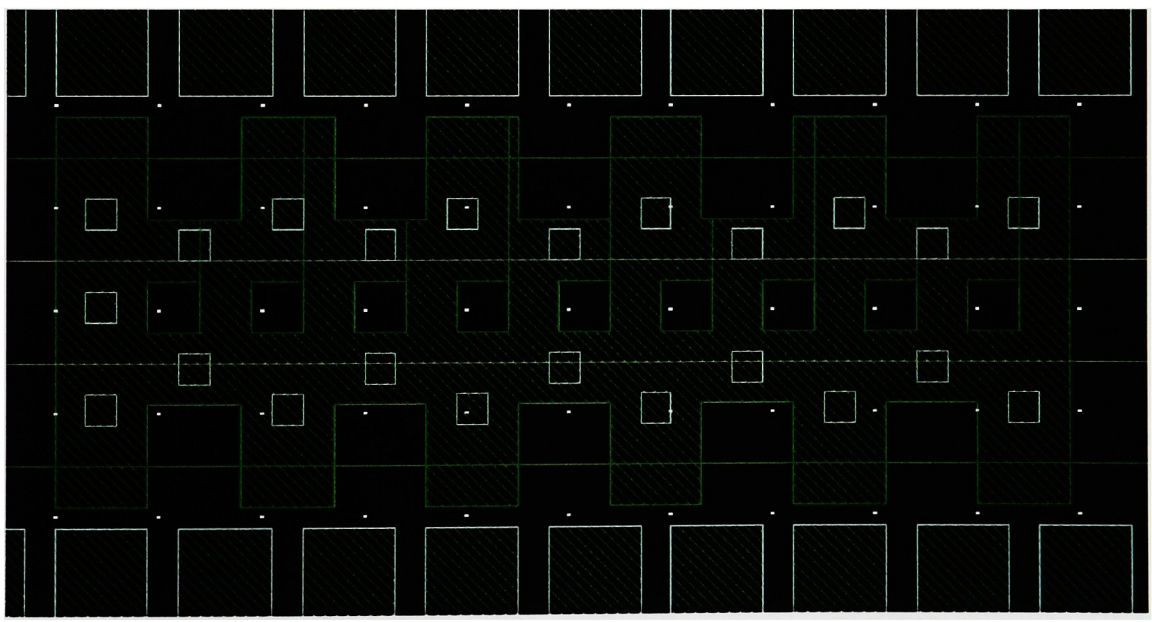

**Figure 47. Mentor Graphic image showing the gray colored squares representing the dimples on the shuttle (Alignment Marks are not shown).**

### 15. Etch Sacrificial Oxide

This step is required to etch sacrificial Oxide from both sides of the track before the third poly deposition can take place. Since the poles (fixed electrodes on both sides of the track) need to be conductive for the device to work, it is important to dope this poly layer.

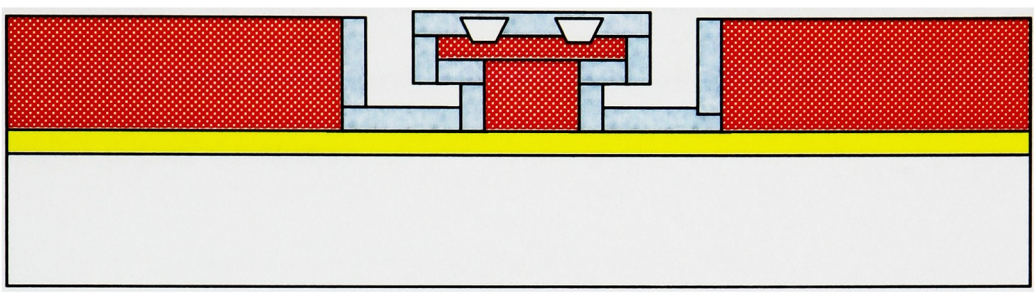

**Figure 48. Etching Sacrificial Oxide to Expose Second Poly**

### 16. Third Poly deposition

This step is the last poly deposition. This third 2-microns thick layer of poly is used to create both the shuttle and the last layer needed to complete the fixed electrodes (stators) on both sides of the track (T-shaped fixed support). This poly silicon layer is 2 microns thick, and it is doped to make it more conductive.

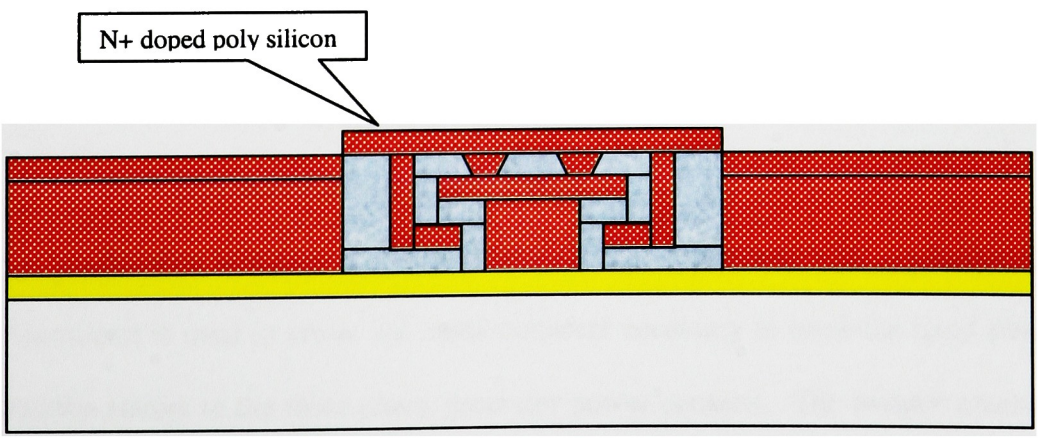


**Figure 49. Third Poly Deposition**

### 17. Etch Poly Silicon

Poly silicon is etched from both sides of the shuttle and windows are created on the shuttle. Windows do not show on this cross sectional area figure. Refer back to the Mentor Graphic design layout (Figure 47) for a detailed view of the windows. The purpose of the windows is to facilitate the sacrificial oxide last etching step to release the shuttle. Dry etch (as described in step 7 above) can be used to etch off the silicon.

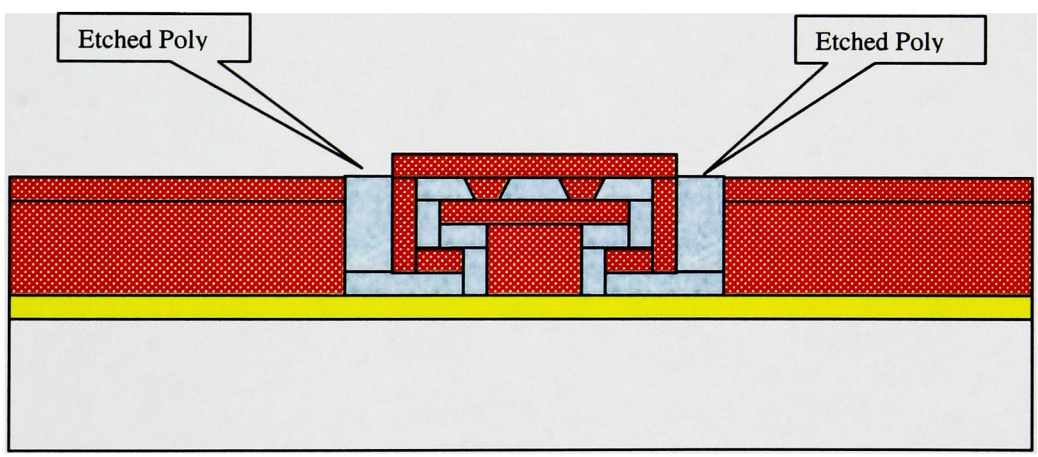


**Figure 50. Etch Third Poly to Get Shuttle Ready for Release**

### 18. Metal deposition and patterning

Another lithography step is used to pattern Aluminum after depositing it. Aluminum is used to create the metal connects necessary to hook the fixed track and the stators to the three-phase generator power contacts. The Mentor graphic

image (Figure 53) shows the metal layer with the three metal connects (A, B, and C) for the different stators, and CC for the fixed track.

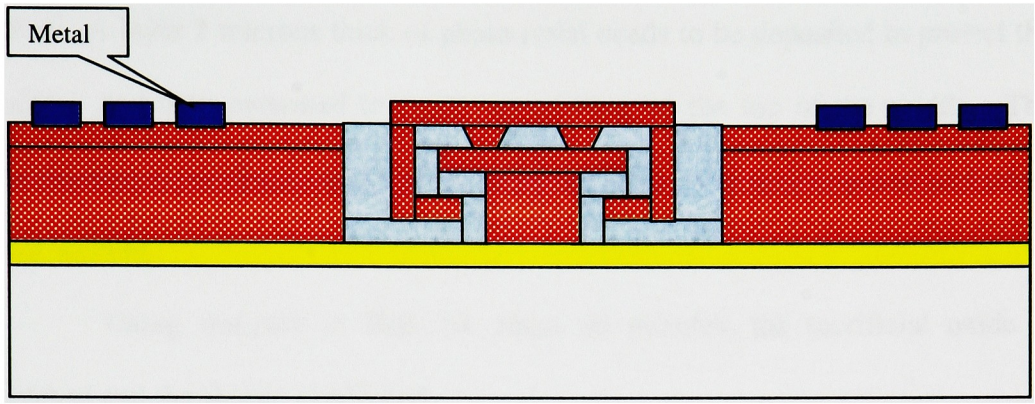


**Figure 51. Metal Deposition and Patterning**

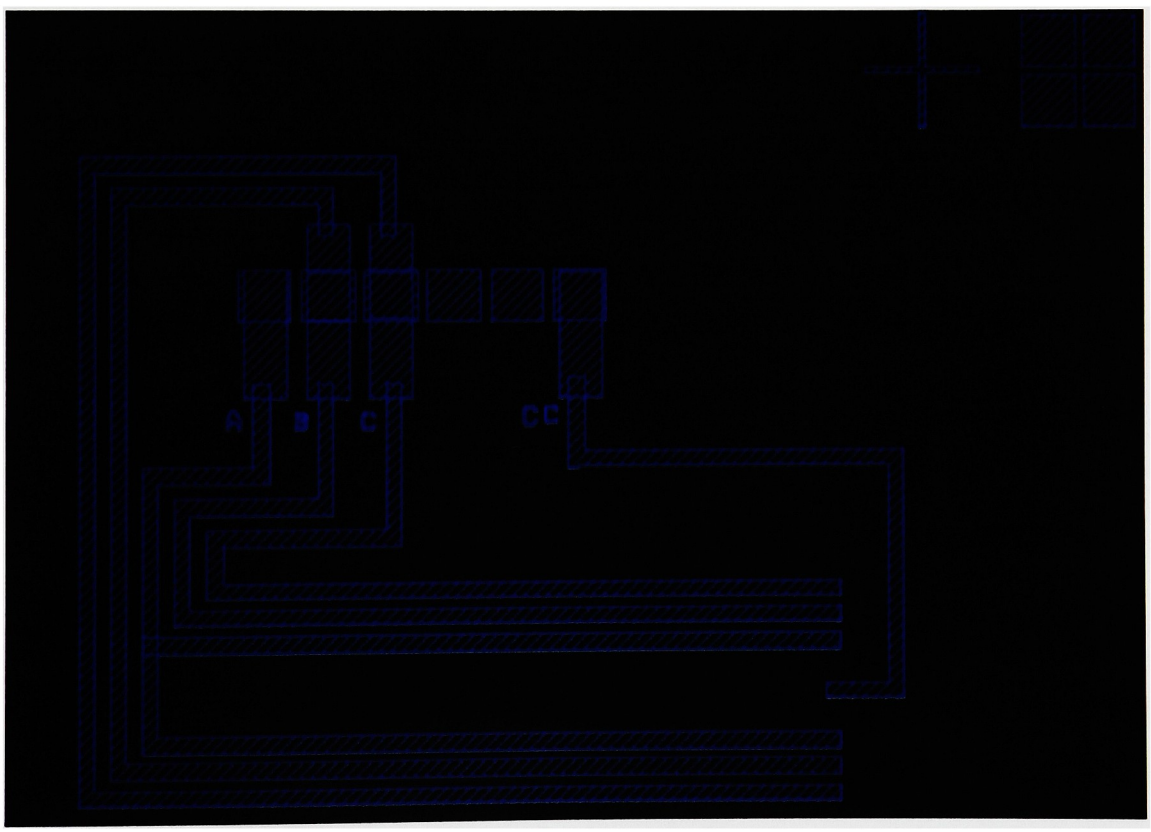


**Figure 52. Layout of the Metal Connects Layer with Alignment Marks Showing**

**19. Release the Shuttle.**

To perform this release step, another lithography step needs to completed first. A layer 2 microns thick of photo resist needs to be deposited to protect the metal, and then patterned to create an opening on the top of the shuttle. The windows on the shuttle and both sides of the shuttle are now exposed and ready for etching.

Using wet-etch in BHF for about 30 minutes, the sacrificial oxide is etched and the shuttle is released.

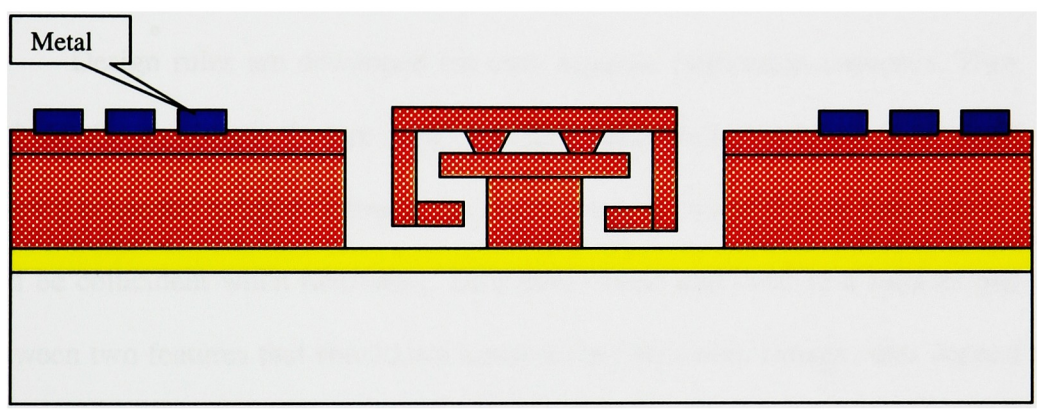


**Figure 53. Release the Shuttle**

## 4.5. Mask Design

### 4.5.1. Mask Design

The concept of a "minimum feature size" is important in mask design. The minimum feature size is the width of the smallest line or gap that appears in the design. When the mask is produced, the minimum feature size will be required to set up the equipment. A small minimum feature size will mean that the mask

creation process takes a long time and becomes increasingly expensive; with very small features (sub-micron) it may be necessary to perform additional processing of the mask for optical correction purposes. This should not happen for most micromachining applications, however: one would expect to have minimum feature sizes in the region of a few micrometers.

In this design, the smallest feature size is 2 microns; therefore, it is not of any concern to us to worry about the minimum feature size.

### 4.5.2. Design Rules

Design rules are developed for each separate fabrication sequence. They include the minimum feature size, but they, essentially, indicate how much overlap is needed to leave between two mask layers to ensure that the two features will be coincident when fabricated. They also ensure that there is a suitable gap between two features that should not touch when fabricated. Design rules depend upon the expected alignment error that will be introduced during fabrication. This will be comparatively large when doing double-sided alignment. If we take an arbitrary value of +/- 1 micron alignment error, for example, and we wish to etch a via hole over a metal pad, then it would be wise to leave at least an underlap (gap) of at least 2 microns.

Many mask design software packages come with design rule checkers, which will automatically check your design against the rules that you enter, and highlight any deviation from the rules [30].

The smallest feature size in this design is 2 microns, which poses some questions regarding the possibility of having small tolerances. In other words, in the proposed design, an error of 2 microns, which is possible, is not desirable. The gap between the shuttle and the fixed support (track), and also the gap between the fixed electrodes (Poles) and the shuttle is 2 microns.

# Chapter V: Conclusions and Recommendations

## 5.1. Conclusions

MEMS devices today come in different shapes and forms from sensors, transducers, and accelerometers which can measure things like stress, pressure, temperature, etc. to linear and rotary motors, and even gas turbines. Some of the fastest growing are rf MEMS for wireless devices and bioMEMS (lab-on-a-chip) that can perform DNA analysis. There seems to be a continuous increase in the number and variety of applications in which microelectromechanical systems are applied or have the potential to be useful. Different types of micromotors especially rotary and wobble motors have been studied, fabricated, and tested in different environments, under a mixture of conditions and for the purpose of exploitation in diverse applications.

Laterally driven micromotors and linear motion microactuators have also been fabricated and researched, although not as extensively; their use have been studied in different applications. Concepts such as piezoelectric (produces ultrasonic vibrations in a stator structure, which can lead to linear motion), inchworm, and high-speed stepper motors have been developed. The driving force for such variety of motors is more often than not either electrostatic or electromagnetic. Electrostatically driven motors are usually faster and easier to fabricate than their electromagnetic counterparts. Electrostatic actuation is the most frequently applied principle combining versatility and simple technology. It needs neither additional elements like coils or cores, as it is the case for electromagnetic actuators, nor special materials like shape-memory-alloys or piezoelectric

ceramics. Moreover, electrostatic microactuators can travel much larger displacements during a linear motion than say piezoelectric ones.

The device, which is the subject of the study in this thesis, is a long distance traveling microactuator. The principle force of operation for this stepper motor is electrostatic. The objective of this work was to demonstrate analytically and through modeling that the concept of such a device is feasible. It was also the goal of this experimental study to develop a flow process that is suitable for the manufacturing of such a device in the future. The principle of operation of this device, although seems to be relatively simple, has never been considered for research before this attempt. Similar concepts, however, have been addressed in the literature in the past. This device as it was explained before has three main components, which are the shuttle (moving electrode), fixed track (shuttle support), and the fixed electrodes (stators).

All the significant forces exerted on this device and all the variables and parameters, which describe the environment and conditions in which this device is to be simulated in, have been considered and incorporated in the dynamic modeling of the device. Magnetic forces and fringing fields were neglected, because they were insignificant in comparison to electrostatic forces generated. Friction between the rough surfaces in contact has been assumed to have the largest kinetic coefficient as a worst-case scenario to be studied in the dynamic modeling of the device. So, for all the calculations performed using a potential difference range of five to thirty volts, a value of 5 (highest) for the kinetic of friction coefficient was used. Under normal conditions of pressure and

temperature, and upon the application of a bias voltage of ranges from 5 to 30 volts it was found that enough electrostatic force is generated to overcome all the friction and drag forces and propel the device. By design, continuous motion of the shuttle is pragmatic when a three-phase voltage driver is used to power the device. The displacement of the shuttle was shown to linearly increase as a function of time, and the shuttle covered a distance of about 1000 microns (length of the designed track) in roughly a few milliseconds. The lowest and highest values for the velocity calculated are 1.10 m/s, and 11.16 m/s respectively, achieved when voltages of 5 and 30 were applied in that order. These speeds are typical of similar devices operating with comparable voltage values. Of course, for any applications of such a device where carrying a load is important, larger voltage values would need to be applied in order to get the shuttle moving. These values could be easily determined if the weight, size, and structure of the load is known.

A process flow was also developed and all the different steps necessary to fabricate this device were discussed in detail. It is important to note that there are several ways such a manufacturing process could be approached. There are different deposition and etching methods, as well as different lithography steps that could be arranged and chosen in a fashion, which would minimize the processing time, and human made errors without compromising the integrity of the device. The capabilities of manufacturing that RIT has were taken in consideration when this process was developed. The concept for the electrostatically driven long distance traveling microactuator is feasible as it has

been analytically proven and it is also realistic to develop and manufacture such a device.

## 5.2. Recommendations

The next logical step in this endeavor is to use the flow process developed earlier in this study and fabricate the device. Several dozen devices should be manufactured simultaneously. Surface micro-machining technology allows such relative mass production to happen. It is important to observe caution and be very careful when performing the different fabrication processes, since some processes are irreversible and one error could render the whole device inoperable. Such a mishap usually means starting over from scratch, which could be time consuming and costly. A more professional job could be done with better results if the work of manufacturing the device is outsourced to a specialized company in the fabrication of MEMS devices. This option can prove to be costly, but could save time and avoid expensive mistakes, which could occur if it is opted to manufacture the device locally (RIT). Testing needs then to take place on several devices randomly chosen, if not all the manufactured devices. The test results are important to confirm the analytically obtained results.

Depending on the application this device is going to be used in and how long it has to operate, some lubricant needs to be applied to minimize friction and wear of the dimples, which are the main points of contact between the shuttle and the track. The experimenter should try with different liquid lubricants, such as the bonded Z-DOL, or bathing the device in the customary silicone oil, which provides several expected benefits. There is a tradeoff, however, when a liquid

lubricant is applied and that is the speed of operation of the micromotor is reduced significantly because of the large viscous drag forces caused by the liquid medium. So, depending on the application if relatively low speed is desired, then liquid lubrication is a good solution to wear and reliable start-up caused by stiction and meniscus. On the other hand if high-speed operation is desired, then dry lubricants are an option to be considered, although they are difficult to control and their application to such micro-device can be problematic, because the size of the microdevice is in the order of the particles size in some lubricants.

There are a number of applications, such as the ones mentioned in the introduction, where a linear long distance traveling microactuator could be used. Depending on the nature of the application proper care in designing or modifying the process flow should be taken, appropriate testing must be performed, and the right lubrication ought to be applied in order to insure long lasting operation, nominal wear, and suitable function of the device.

# REFERENCES


[1] H.C. Nathanson, et al., The Resonant Gate Transistor, IEEE Trans. Electron Devices, March 1967, Vol. 14, no. 3, pp 117-133

[2] E. Thielicke, E. Obermeier. Microactuators and their Technologies Technical University of Berlin, Microsensor & -actuator Technology Center (MAT)

[3] Sergey Edward Lyshevski. MEMS and NEMS Systems, Devices, and Structures, CRC Press 2002.

[4] MEMS Clearinghouse by MEMS Exchange 2003. http://www.memsnet.org

[5] Future Applications of Micro/Nano-Technologies in Space Systems. ESA Bulletin Nr. 85. 1996. http://esapub.esrin.esa.it/bulletin/bullet85/mart85.htm

[6] Ernst Thielicke, Ernst Obermeier. Microatuators and their technologies. Technical University of Berlin, Microsensor and Microactuator Technology Center (MAT), TIB 3.1, Gustav-Meyer-Allee 25, 13355, Berlin, Germany

[7] Prosenjit Rai-Choudhury. MEMS and MOEMS Technology and Applications. P. cm. SPIE Press Monograph; Volume PM85.

[8] Frank L. H. Wolfs. Effects of one point on a charged surface, University of Rochester, NY 14627

[9] Jay Y. Zhao. Louisiana Tech. MEMS Dissertation draft, www2.latech.edu/~yzh007/mems

[10] M.C. Elwenspoek, MICMEC, http://utep.el.utwente.nl/tdm/mmd/projects/combs/

[11] Electrostatic Actuators, W.C. Tang, etal. T. Hirano, T. Furuhata, K.J. Gabriel (UCLA)

[12] Xingtao Wu, Jiang Zhe, Jingshan Wang, Jin Cheng, Vijay Modi, and K. R. Farmer. A generalized capacitance-based model for electrostatic micro-actuators. Department of Physics, New Jersey Institute of Technology, Newark, NJ, Department of Mechanical Engineering, Columbia University, NY

[13] Sriram Sundararajan, Bharat Bhushan. Micro/nanotribological studies of polysilicon and SiC films for MEMS applications. Wear 217 (1998) 251-261

[14] M. Kohl, J. Gottert, J. Mohr. Verification of the micromechanical characteristics of electrostatic linear actuators. Sensors and Actuators A 53 (1996) 416-422

[15] Omar M P, Mehregany M, and Mullen R L. Electric and fluid field analysis of side-drive micromotors. J. Microelectromech. Microsyst. 1 1992.

[16] Mohd P. Omar, Merhan Mehregany, Member, IEEE, and Robert L. Mullen. Electric and Fluid Analysis of Side-Drive Micromotors. Journal of microelectromechanical systems. VOL. 1. NO. 3. September 1992

[17] Robert L. Mott. Applied Fluid Mechanics, Fifth Edition, 2000 Prentice-Hall, Inc.

[18] John D. Anderson, Jr. Modern Compressible Flow with Historian Perspective, second edition. McGraw Hill, Inc. 1990

[19] Michael J. Martin, Katsuo Kurabayashi University of Michigan Department of Mechanical Engineering, Iain D. Boyd. Measurement of Lift and Drag on MEMS scale airfoils in Slip Flow. Proceedings of ASME FEDSM.01 2001 ASME Fluids Engineering Division Summer Meeting New Orleans, Louisiana, May 29-June 1, 2001.

[20] Warren F. Phillips, Mechanics of Flight. John Wiley & Sons, Inc. Hoboken, New Jersey, 2004

[21] Frank M. White, Fluid Mechanics, Fourth Edition. The McGraw Hill companies, Inc. 1999.

[22] Sriram Sundararajan, Bharat Bhushan. Static friction and surface roughness studies of surface micromachined electrostatic micromotors using an atomic force/friction force microscope. January 2001

[23] Susan M. Lea, John Robert Burke. Physics The Nature of Things. West Publishing Company, 1997

[24] Chih-Ming Ho, Yu-Chong Tai. Micro-Electro-Mechanical Systems (MEMS) and Fluid Flows. Annu. Rev. Fluid Mech. 1998. 30:579–612

[25] M.Esashi. Silicon bulk micromachining. New Industry Creation Hatchery Center, Tohoku University, Sendai, 980-8579, Japan (referenced by: http://trimmer.net/)

[26] Kenneth Breuer. Lubrication in MEMS. CRC Handbook on MEMS Ed. M. Gad el Hak, CRC Press 2001

[27] S.L. Miller, J.J. Sniegowski, G. LaVigne, and P.J. McWhorter. Friction in surface micromachined microengines. Sandia National Laboratories, Albuquerque, NM.

[28] B. Bhushan, Principles and Applications of Tribology (Wiley, New York, 1999)

[29] Lynn F. Fuller, Bulk Micromachined Pressure Sensor, ppt lecture. June 2003.

[30] Danny Banks, 5 June 1999. http://www.dbanks.demon.co.uk

# Appendix A- Tables of Data and Results of Calculations

The following symbols are used in the tables below to calculate the displacement, velocity, and friction and drag forces for different values of the voltage and kinetic coefficient of friction:

* x: Displacement
* x': Velocity
* V: Voltage
* mu(k): Kinetic Coefficient of friction
* P: Variable defined above in section 2.3.1 to simplify calculations
* D: Variable defined above in section 2.3.1 to simplify calculations
* Theta (θ): Variable defined above in section 2.3.1 to simplify calculations
* $F_C$: Friction Forces
* $F_D$: Drag Forces
* sqrt(): Square root

| sqrt (P) | 1-sqrt(P) | mu (k) | V | D | sqrt(D) | m | Theta | sqrt(D)/sqrt(P) | m/p |
|---|---|---|---|---|---|---|---|---|---|
| 4.36922E-05 | 0.999956308 | 5 | 5 | 2.34045E-09 | 4.83782E-05 | 1.99044*10^-11 | 212.3901931 | 1.107249719 | 0.010426561 |
| | | | | | | | | | |
| t | x5(t) | x'5(t) | | Fc+FD | x10(t) | x'10(t) | Fc+FD (10 v) | x15 (t) | x'15(t) |
| 0.0000 | 2.08531E-12 | 1.107152963 | | 3.31834E-09 | 2.08531E-12 | 2.537770394 | 1.32728E-08 | 2.08531E-12 | 3.889871041 |
| 0.0001 | 0.000110715 | 1.107154996 | | 3.31835E-09 | 0.000253777 | 2.537780932 | 1.32729E-08 | 0.000388988 | 3.889895484 |
| 0.0002 | 0.000221431 | 1.107156986 | | 3.31836E-09 | 0.000507556 | 2.537790969 | 1.3273E-08 | 0.000777979 | 3.889918169 |
| 0.0003 | 0.000332147 | 1.107158935 | | 3.31837E-09 | 0.000761336 | 2.53780053 | 1.32731E-08 | 0.001166972 | 3.889939223 |
| 0.0004 | 0.000442863 | 1.107160843 | | 3.31837E-09 | 0.001015116 | 2.537809636 | 1.32732E-08 | 0.001555966 | 3.889958764 |
| 0.0005 | 0.000553579 | 1.107162711 | | 3.31838E-09 | 0.001268897 | 2.537818309 | 1.32733E-08 | 0.001944963 | 3.889976899 |
| 0.0006 | 0.000664295 | 1.107164539 | | 3.31839E-09 | 0.001522679 | 2.537826571 | 1.32734E-08 | 0.002333961 | 3.889993731 |
| 0.0007 | 0.000775012 | 1.107166329 | | 3.3184E-09 | 0.001776462 | 2.537834439 | 1.32735E-08 | 0.002722961 | 3.890009352 |
| 0.0008 | 0.000885728 | 1.107168081 | | 3.3184E-09 | 0.002030246 | 2.537841934 | 1.32735E-08 | 0.003111963 | 3.89002385 |
| 0.0009 | 0.000996445 | 1.107169797 | | 3.31841E-09 | 0.002284031 | 2.537849073 | 1.32736E-08 | 0.003500966 | 3.890037306 |
| 0.0010 | 0.001107162 | 1.107171476 | | 3.31842E-09 | 0.002537816 | 2.537855873 | 1.32737E-08 | 0.00388997 | 3.890049794 |
| 0.0011 | 0.001217879 | 1.107173121 | | 3.31843E-09 | 0.002791602 | 2.537862349 | 1.32737E-08 | 0.004278976 | 3.890061384 |
| 0.0012 | 0.001328597 | 1.10717473 | | 3.31843E-09 | 0.003045388 | 2.537868518 | 1.32738E-08 | 0.004667982 | 3.890072141 |
| 0.0013 | 0.001439314 | 1.107176306 | | 3.31844E-09 | 0.003299175 | 2.537874394 | 1.32739E-08 | 0.00505699 | 3.890082124 |
| 0.0014 | 0.001550032 | 1.107177849 | | 3.31845E-09 | 0.003552963 | 2.53787999 | 1.32739E-08 | 0.005445998 | 3.89009139 |
| 0.0015 | 0.00166075 | 1.107179359 | | 3.31845E-09 | 0.003806751 | 2.537885321 | 1.3274E-08 | 0.005835008 | 3.890099989 |
| 0.0016 | 0.001771468 | 1.107180838 | | 3.31846E-09 | 0.00406054 | 2.537890398 | 1.3274E-08 | 0.006224018 | 3.89010797 |
| 0.0017 | 0.001882186 | 1.107182285 | | 3.31846E-09 | 0.004314329 | 2.537895234 | 1.32741E-08 | 0.006613029 | 3.890115377 |
| 0.0018 | 0.001992904 | 1.107183702 | | 3.31847E-09 | 0.004568119 | 2.53789984 | 1.32741E-08 | 0.007002041 | 3.890122252 |
| 0.0019 | 0.002103623 | 1.10718509 | | 3.31848E-09 | 0.004821909 | 2.537904228 | 1.32741E-08 | 0.007391053 | 3.890128632 |
| 0.0020 | 0.002214341 | 1.107186448 | | 3.31848E-09 | 0.005075699 | 2.537908407 | 1.32742E-08 | 0.007780066 | 3.890134554 |
| 0.0021 | 0.00232506 | 1.107187777 | | 3.31849E-09 | 0.00532949 | 2.537912387 | 1.32742E-08 | 0.00816908 | 3.89014005 |
| 0.0022 | 0.002435779 | 1.107189079 | | 3.31849E-09 | 0.005583282 | 2.537916178 | 1.32743E-08 | 0.008558094 | 3.89014515 |
| 0.0023 | 0.002546498 | 1.107190353 | | 3.3185E-09 | 0.005837073 | 2.53791979 | 1.32743E-08 | 0.008947109 | 3.890149884 |
| 0.0024 | 0.002657217 | 1.107191601 | | 3.3185E-09 | 0.006090865 | 2.537923229 | 1.32743E-08 | 0.009336124 | 3.890154277 |
| 0.0025 | 0.002767936 | 1.107192822 | | 3.31851E-09 | 0.006344658 | 2.537926505 | 1.32744E-08 | 0.009725139 | 3.890158355 |
| 0.0026 | 0.002878655 | 1.107194018 | | 3.31851E-09 | 0.00659845 | 2.537929626 | 1.32744E-08 | 0.010114155 | 3.890162139 |
| 0.0027 | 0.002989374 | 1.107195188 | | 3.31852E-09 | 0.006852244 | 2.537932598 | 1.32744E-08 | 0.010503172 | 3.890165651 |
| 0.0028 | 0.003100094 | 1.107196334 | | 3.31852E-09 | 0.007106037 | 2.537935429 | 1.32744E-08 | 0.010892188 | 3.890168911 |
| 0.0029 | 0.003210814 | 1.107197456 | | 3.31853E-09 | 0.00735983 | 2.537938125 | 1.32745E-08 | 0.011281205 | 3.890171936 |
| 0.0030 | 0.003321533 | 1.107198554 | | 3.31853E-09 | 0.007613624 | 2.537940693 | 1.32745E-08 | 0.011670222 | 3.890174744 |
| 0.0031 | 0.003432253 | 1.10719963 | | 3.31854E-09 | 0.007867418 | 2.537943139 | 1.32745E-08 | 0.01205924 | 3.89017735 |
| 0.0032 | 0.003542973 | 1.107200682 | | 3.31854E-09 | 0.008121213 | 2.537945469 | 1.32745E-08 | 0.012448258 | 3.890179769 |
| 0.0033 | 0.003653693 | 1.107201713 | | 3.31855E-09 | 0.008375007 | 2.537947689 | 1.32746E-08 | 0.012837275 | 3.890182013 |
| 0.0034 | 0.003764414 | 1.107202722 | | 3.31855E-09 | 0.008628802 | 2.537949803 | 1.32746E-08 | 0.013226294 | 3.890184096 |
| 0.0035 | 0.003875134 | 1.107203709 | | 3.31856E-09 | 0.008882597 | 2.537951816 | 1.32746E-08 | 0.013615312 | 3.89018603 |
| 0.0036 | 0.003985854 | 1.107204676 | | 3.31856E-09 | 0.009136392 | 2.537953734 | 1.32746E-08 | 0.014004331 | 3.890187824 |
| 0.0037 | 0.004096575 | 1.107205623 | | 3.31856E-09 | 0.009390188 | 2.53795556 | 1.32746E-08 | 0.014393349 | 3.89018949 |
| 0.0038 | 0.004207295 | 1.107206549 | | 3.31857E-09 | 0.009643983 | 2.5379573 | 1.32747E-08 | 0.014782368 | 3.890191035 |
| 0.0039 | 0.004318016 | 1.107207457 | | 3.31857E-09 | 0.009897779 | 2.537958957 | 1.32747E-08 | 0.015171387 | 3.89019247 |
| 0.0040 | 0.004428737 | 1.107208345 | | 3.31858E-09 | 0.010151575 | 2.537960536 | 1.32747E-08 | 0.015560407 | 3.890193801 |
| 0.0041 | 0.004539458 | 1.107209214 | | 3.31858E-09 | 0.010405371 | 2.537962039 | 1.32747E-08 | 0.015949426 | 3.890195037 |

| | | | | | | | | |
|---|---|---|---|---|---|---|---|---|
| 0.0042 | 0.004650179 | 1.107210065 | 3.31858E-09 | 0.010659167 | 2.537963471 | 1.32747E-08 | 0.016338445 | 3.890196183 |
| 0.0043 | 0.0047609 | 1.107210899 | 3.31859E-09 | 0.010912964 | 2.537964835 | 1.32747E-08 | 0.016727465 | 3.890197248 |
| 0.0044 | 0.004871621 | 1.107211714 | 3.31859E-09 | 0.01116676 | 2.537966134 | 1.32747E-08 | 0.017116484 | 3.890198236 |
| 0.0045 | 0.004982342 | 1.107212513 | 3.31859E-09 | 0.011420557 | 2.537967372 | 1.32748E-08 | 0.017505504 | 3.890199152 |
| 0.0046 | 0.005093063 | 1.107213295 | 3.3186E-09 | 0.011674353 | 2.53796855 | 1.32748E-08 | 0.017894524 | 3.890200003 |
| 0.0047 | 0.005203784 | 1.10721406 | 3.3186E-09 | 0.01192815 | 2.537969673 | 1.32748E-08 | 0.018283544 | 3.890200793 |
| 0.0048 | 0.005314506 | 1.10721481 | 3.3186E-09 | 0.012181947 | 2.537970742 | 1.32748E-08 | 0.018672564 | 3.890201526 |
| 0.0049 | 0.005425227 | 1.107215543 | 3.31861E-09 | 0.012435744 | 2.53797176 | 1.32748E-08 | 0.019061584 | 3.890202206 |
| 0.0050 | 0.005535949 | 1.107216262 | 3.31861E-09 | 0.012689541 | 2.53797273 | 1.32748E-08 | 0.019450604 | 3.890202837 |

| x20(t) | x'20(t) |
|---|---|
| 2.08531E-12 | 5.224771969 |
| 0.000522479 | 5.224815513 |
| 0.001044963 | 5.224854905 |
| 0.00156745 | 5.22489054 |
| 0.002089941 | 5.224922778 |
| 0.002612434 | 5.22495194 |
| 0.003134931 | 5.224978322 |
| 0.00365743 | 5.225002188 |
| 0.004179931 | 5.225023778 |
| 0.004702434 | 5.225043309 |
| 0.00522494 | 5.225060977 |
| 0.005747446 | 5.22507696 |
| 0.006269955 | 5.225091419 |
| 0.006792465 | 5.225104499 |
| 0.007314976 | 5.225116332 |
| 0.007837488 | 5.225127036 |
| 0.008360001 | 5.22513672 |
| 0.008882515 | 5.225145479 |
| 0.00940503 | 5.225153404 |
| 0.009927545 | 5.225160573 |
| 0.010450062 | 5.225167058 |
| 0.010972579 | 5.225172924 |
| 0.011495096 | 5.225178231 |
| 0.012017614 | 5.225183032 |
| 0.012540133 | 5.225187375 |
| 0.013062651 | 5.225191304 |
| 0.013585171 | 5.225194859 |
| 0.01410769 | 5.225198074 |
| 0.01463021 | 5.225200982 |
| 0.01515273 | 5.225203614 |
| 0.015675251 | 5.225205994 |
| 0.016197771 | 5.225208147 |
| 0.016720292 | 5.225210095 |
| 0.017242813 | 5.225211857 |
| 0.017765335 | 5.225213451 |
| 0.018287856 | 5.225214893 |

| | |
|---|---|
| 0.018810377 | 5.225216198 |
| 0.019332899 | 5.225217378 |
| 0.019855421 | 5.225218446 |
| 0.020377943 | 5.225219411 |
| 0.020900464 | 5.225220285 |
| 0.021422986 | 5.225221075 |
| 0.021945509 | 5.22522179 |
| 0.022468031 | 5.225222437 |
| 0.022990553 | 5.225223022 |
| 0.023513075 | 5.225223551 |
| 0.024035597 | 5.22522403 |
| 0.02455812 | 5.225224463 |
| 0.025080642 | 5.225224855 |
| 0.025603165 | 5.22522521 |
| 0.026125687 | 5.22522553 |

| sqrt (P) | 1-sqrt(P) | mu (k) | V | D | sqrt(D) | m | Theta | sqrt(D)/sqrt(P) | m/p |
|---|---|---|---|---|---|---|---|---|---|
| 4.36922E-05 | 0.999956308 | 5 | 10 | 1.22967E-08 | 0.00011089 | 1.99044*10^-11 | 486.8320475 | 2.537992175 | 0.010426561 |

| t | x10(t) | x'10(t) | | Fc+FD (10 v) |
|---|---|---|---|---|
| 0.0000 | 2.08531E-12 | 2.537770394 | | 1.32728E-08 |
| 0.0001 | 0.000253777 | 2.537780932 | | 1.32729E-08 |
| 0.0002 | 0.000507556 | 2.537790969 | | 1.3273E-08 |
| 0.0003 | 0.000761336 | 2.53780053 | | 1.32731E-08 |
| 0.0004 | 0.001015116 | 2.537809636 | | 1.32732E-08 |
| 0.0005 | 0.001268897 | 2.537818309 | | 1.32733E-08 |
| 0.0006 | 0.001522679 | 2.537826571 | | 1.32734E-08 |
| 0.0007 | 0.001776462 | 2.537834439 | | 1.32735E-08 |
| 0.0008 | 0.002030246 | 2.537841934 | | 1.32735E-08 |
| 0.0009 | 0.002284031 | 2.537849073 | | 1.32736E-08 |
| 0.0010 | 0.002537816 | 2.537855873 | | 1.32737E-08 |
| 0.0011 | 0.002791602 | 2.537862349 | | 1.32737E-08 |
| 0.0012 | 0.003045388 | 2.537868518 | | 1.32738E-08 |
| 0.0013 | 0.003299175 | 2.537874394 | | 1.32739E-08 |
| 0.0014 | 0.003552963 | 2.53787999 | | 1.32739E-08 |
| 0.0015 | 0.003806751 | 2.537885321 | | 1.3274E-08 |
| 0.0016 | 0.00406054 | 2.537890398 | | 1.3274E-08 |
| 0.0017 | 0.004314329 | 2.537895234 | | 1.32741E-08 |
| 0.0018 | 0.004568119 | 2.53789984 | | 1.32741E-08 |
| 0.0019 | 0.004821909 | 2.537904228 | | 1.32741E-08 |
| 0.0020 | 0.005075699 | 2.537908407 | | 1.32742E-08 |
| 0.0021 | 0.00532949 | 2.537912387 | | 1.32742E-08 |
| 0.0022 | 0.005583282 | 2.537916178 | | 1.32743E-08 |
| 0.0023 | 0.005837073 | 2.53791979 | | 1.32743E-08 |
| 0.0024 | 0.006090865 | 2.537923229 | | 1.32743E-08 |
| 0.0025 | 0.006344658 | 2.537926505 | | 1.32744E-08 |

| | | | | |
|---|---|---|---|---|
| 0.0026 | 0.00659845 | 2.537929626 | | 1.32744E-08 |
| 0.0027 | 0.006852244 | 2.537932598 | | 1.32744E-08 |
| 0.0028 | 0.007106037 | 2.537935429 | | 1.32744E-08 |
| 0.0029 | 0.00735983 | 2.537938125 | | 1.32745E-08 |
| 0.0030 | 0.007613624 | 2.537940693 | | 1.32745E-08 |
| 0.0031 | 0.007867418 | 2.537943139 | | 1.32745E-08 |
| 0.0032 | 0.008121213 | 2.537945469 | | 1.32745E-08 |
| 0.0033 | 0.008375007 | 2.537947689 | | 1.32746E-08 |
| 0.0034 | 0.008628802 | 2.537949803 | | 1.32746E-08 |
| 0.0035 | 0.008882597 | 2.537951816 | | 1.32746E-08 |
| 0.0036 | 0.009136392 | 2.537953734 | | 1.32746E-08 |
| 0.0037 | 0.009390188 | 2.53795556 | | 1.32746E-08 |
| 0.0038 | 0.009643983 | 2.5379573 | | 1.32747E-08 |
| 0.0039 | 0.009897779 | 2.537958957 | | 1.32747E-08 |
| 0.0040 | 0.010151575 | 2.537960536 | | 1.32747E-08 |
| 0.0041 | 0.010405371 | 2.537962039 | | 1.32747E-08 |
| 0.0042 | 0.010659167 | 2.537963471 | | 1.32747E-08 |
| 0.0043 | 0.010912964 | 2.537964835 | | 1.32747E-08 |
| 0.0044 | 0.01116676 | 2.537966134 | | 1.32747E-08 |
| 0.0045 | 0.011420557 | 2.537967372 | | 1.32748E-08 |
| 0.0046 | 0.011674353 | 2.53796855 | | 1.32748E-08 |
| 0.0047 | 0.01192815 | 2.537969673 | | 1.32748E-08 |
| 0.0048 | 0.012181947 | 2.537970742 | | 1.32748E-08 |
| 0.0049 | 0.012435744 | 2.53797176 | | 1.32748E-08 |
| 0.0050 | 0.012689541 | 2.53797273 | | 1.32748E-08 |

| sqrt (P) | 1-sqrt(P) | mu (k) | V | D | sqrt(D) | m | Theta | sqrt(D)/sqrt(P) | m/P |
|---|---|---|---|---|---|---|---|---|---|
| 4.36922E-05 | 0.999956308 | 5 | 15 | 2.88904E-08 | 0.000169972 | 1.99044*10^-11 | 746.21167 | 3.890210985 | 0.010426561 |

| t (s) | x15 (t) | x'15(t) | | Fc+FD (15 volts) | | Fc+FD (20 volts) |
|---|---|---|---|---|---|---|
| 0.0000 | 2.08531E-12 | 3.889871041 | | 2.98637E-08 | | 5.30909E-08 |
| 0.0001 | 0.000388988 | 3.889895484 | | 2.98641E-08 | | 5.30917E-08 |
| 0.0002 | 0.000777979 | 3.889918169 | | 2.98644E-08 | | 5.30925E-08 |
| 0.0003 | 0.001166972 | 3.889939223 | | 2.98647E-08 | | 5.30932E-08 |
| 0.0004 | 0.001555966 | 3.889958764 | | 2.9865E-08 | | 5.30939E-08 |
| 0.0005 | 0.001944963 | 3.889976899 | | 2.98653E-08 | | 5.30945E-08 |
| 0.0006 | 0.002333961 | 3.889993731 | | 2.98655E-08 | | 5.3095E-08 |
| 0.0007 | 0.002722961 | 3.890009352 | | 2.98657E-08 | | 5.30955E-08 |
| 0.0008 | 0.003111963 | 3.89002385 | | 2.9866E-08 | | 5.30959E-08 |
| 0.0009 | 0.003500966 | 3.890037306 | | 2.98662E-08 | | 5.30963E-08 |
| 0.0010 | 0.00388997 | 3.890049794 | | 2.98663E-08 | | 5.30966E-08 |
| 0.0011 | 0.004278976 | 3.890061384 | | 2.98665E-08 | | 5.3097E-08 |
| 0.0012 | 0.004667982 | 3.890072141 | | 2.98667E-08 | | 5.30972E-08 |
| 0.0013 | 0.00505699 | 3.890082124 | | 2.98668E-08 | | 5.30975E-08 |
| 0.0014 | 0.005445998 | 3.89009139 | | 2.9867E-08 | | 5.30977E-08 |
| 0.0015 | 0.005835008 | 3.890099989 | | 2.98671E-08 | | 5.3098E-08 |

| | | | | | | |
|---|---|---|---|---|---|---|
| 0.0016 | 0.006224018 | 3.89010797 | | 2.98672E-08 | | 5.30981E-08 |
| 0.0017 | 0.006613029 | 3.890115377 | | 2.98673E-08 | | 5.30983E-08 |
| 0.0018 | 0.007002041 | 3.890122252 | | 2.98674E-08 | | 5.30985E-08 |
| 0.0019 | 0.007391053 | 3.890128632 | | 2.98675E-08 | | 5.30986E-08 |
| 0.0020 | 0.007780066 | 3.890134554 | | 2.98676E-08 | | 5.30988E-08 |
| 0.0021 | 0.00816908 | 3.89014005 | | 2.98677E-08 | | 5.30989E-08 |
| 0.0022 | 0.008558094 | 3.89014515 | | 2.98678E-08 | | 5.3099E-08 |
| 0.0023 | 0.008947109 | 3.890149884 | | 2.98678E-08 | | 5.30991E-08 |
| 0.0024 | 0.009336124 | 3.890154277 | | 2.98679E-08 | | 5.30992E-08 |
| 0.0025 | 0.009725139 | 3.890158355 | | 2.9868E-08 | | 5.30992E-08 |
| 0.0026 | 0.010114155 | 3.890162139 | | 2.9868E-08 | | 5.30993E-08 |
| 0.0027 | 0.010503172 | 3.890165651 | | 2.98681E-08 | | 5.30994E-08 |
| 0.0028 | 0.010892188 | 3.890168911 | | 2.98681E-08 | | 5.30994E-08 |
| 0.0029 | 0.011281205 | 3.890171936 | | 2.98682E-08 | | 5.30995E-08 |
| 0.0030 | 0.011670222 | 3.890174744 | | 2.98682E-08 | | 5.30995E-08 |
| 0.0031 | 0.01205924 | 3.89017735 | | 2.98682E-08 | | 5.30996E-08 |
| 0.0032 | 0.012448258 | 3.890179769 | | 2.98683E-08 | | 5.30996E-08 |
| 0.0033 | 0.012837275 | 3.890182013 | | 2.98683E-08 | | 5.30996E-08 |
| 0.0034 | 0.013226294 | 3.890184096 | | 2.98683E-08 | | 5.30997E-08 |
| 0.0035 | 0.013615312 | 3.89018603 | | 2.98684E-08 | | 5.30997E-08 |
| 0.0036 | 0.014004331 | 3.890187824 | | 2.98684E-08 | | 5.30997E-08 |
| 0.0037 | 0.014393349 | 3.89018949 | | 2.98684E-08 | | 5.30998E-08 |
| 0.0038 | 0.014782368 | 3.890191035 | | 2.98684E-08 | | 5.30998E-08 |
| 0.0039 | 0.015171387 | 3.89019247 | | 2.98685E-08 | | 5.30998E-08 |
| 0.0040 | 0.015560407 | 3.890193801 | | 2.98685E-08 | | 5.30998E-08 |
| 0.0041 | 0.015949426 | 3.890195037 | | 2.98685E-08 | | 5.30998E-08 |
| 0.0042 | 0.016338445 | 3.890196183 | | 2.98685E-08 | | 5.30998E-08 |
| 0.0043 | 0.016727465 | 3.890197248 | | 2.98685E-08 | | 5.30999E-08 |
| 0.0044 | 0.017116484 | 3.890198236 | | 2.98686E-08 | | 5.30999E-08 |
| 0.0045 | 0.017505504 | 3.890199152 | | 2.98686E-08 | | 5.30999E-08 |
| 0.0046 | 0.017894524 | 3.890200003 | | 2.98686E-08 | | 5.30999E-08 |
| 0.0047 | 0.018283544 | 3.890200793 | | 2.98686E-08 | | 5.30999E-08 |
| 0.0048 | 0.018672564 | 3.890201526 | | 2.98686E-08 | | 5.30999E-08 |
| 0.0049 | 0.019061584 | 3.890202206 | | 2.98686E-08 | | 5.30999E-08 |
| 0.0050 | 0.019450604 | 3.890202837 | | 2.98686E-08 | | 5.30999E-08 |

| sqrt (P) | 1-sqrt(P) | mu (k) | V | D | sqrt(D) | m | Theta | sqrt(D)/sqrt(P) | m/P |
|---|---|---|---|---|---|---|---|---|---|
| 4.36922E-05 | 0.999956308 | 5 | 20 | 5.21217E-08 | 0.000228302 | 1.99044*10^-11 | 1002.291792 | 5.225228572 | 0.010426561 |

| t (s) | x20(t) | x'20(t) | | Fc+FD (20 volts) |
|---|---|---|---|---|
| 0.0000 | 2.08531E-12 | 5.224771969 | | 5.30909E-08 |
| 0.0001 | 0.000522479 | 5.224815513 | | 5.30917E-08 |
| 0.0002 | 0.001044963 | 5.224854905 | | 5.30925E-08 |
| 0.0003 | 0.00156745 | 5.22489054 | | 5.30932E-08 |
| 0.0004 | 0.002089941 | 5.224922778 | | 5.30939E-08 |
| 0.0005 | 0.002612434 | 5.22495194 | | 5.30945E-08 |